Effects of Temperature, Humidity, Nitrogen Dioxide and Nitric Acid Gases on Carbon-Steel, Galvanized, and Painted Steel

Final Report

Prepared for the California Air Resources Board

Agreement A4-109-32

M.R. Whitbeck

Desert Research Institute
University of Nevada

D.A. Jones

University of Nevada at Reno

August 1987

Disclaimer

The statements and conclusions in this report are those of the contractor and not necessarily those of the California Air Resources Board. The mention of commercial products, their source or their use in connection with material reported herein is not to be construed as either an actual or implied endorsement of such products.

Abstract

The objective of this study is to investigate the potential effect of nitrogen dioxide and nitric acid on carbon–steel, galvanized and painted steel under initial exposure conditions. This study attempts to measure initial rates of corrosion at realistically short times using techniques less ambiguous than weight loss/gain methods employed with longer exposure times.

Surface electrode microcells were developed to directly show the effects of humidity and pollutant nitrogen dioxide and nitric acid gases on metals without requiring wetted surfaces. Corrosion is an electrochemical phenomenon and these miniature electrochemical cells measure corrosion rate more directly and more sensitively than can be done with bulk weight change. The technique used in this study is called the galvanostatic polarization method and has been used to study the corrosion of wetted metal surfaces, but this is the first application to metal corrosion by gases.

Fourier transform infrared spectroscopy was used to identify surface corrosion products.

Coated galvanized steel sheet was selected for study because it is commonly used for exterior siding in residential and commercial buildings throughout the United States.

Bare steel samples were produced by pickling galvanized coupons in concentrated nitric acid followed by surface abrasion.

Nitrogen dioxide is only a mild corrodant of steel and zinc under the conditions studied. The initial rate of surface degradation is linear in nitrogen dioxide concentration. At the earliest exposure times nitrogen dioxide may weakly passivate (inhibit) corrosion by water vapor. The corrosion products included the metal oxides and nitrate ion. Exposure of the zinc surface to nitrogen dioxide also produced ammonium ion; consistent with the strong reducing power of zinc.

Nitrogen dioxide caused no perceptible damage to the polyester/epoxy painted surfaces under the initial exposure conditions of this study.

Nitric acid gas rapidly attacked both steel and zinc surfaces producing nitrate ions, nitrite ions, and for the zinc surface ammonium ions were also formed.

There was slight degradation of the polyester/epoxy paint surface by nitric acid producing nitrate ester.

Infrared analysis of the surface corrosion products illustrates the nature of the surface alterations. For the pollutants used in this study, ammonium salts were formed which exhibit hygroscopic properties. Hygroscopic salts, which take up water vapor from air, increase the time of wetness of exposed metal surfaces.

The mild damage to the polyester paint by nitric acid may soften the coating lowering its scratch resistance. This, in turn, would promote undercutting by corrosion.

It is recommended that similar studies to these be undertaken using a matrix of humidity, nitrogen dioxide, and sulfur dioxide exposure conditions. The objectives of such studies should be: 1) to determine the nature and extent of the synergism between nitrogen dioxide and sulfur dioxide; 2) to establish the conditions for extending the use of the surface microcells to field studies; 3) to determine the effects of alternate wetting; and 4) to determine the effects of sunlight.

Table of Contents

List of Figures

Glossary

FTIR
: Fourier Transform Infrared spectrometer, a device for measuring infrared spectra.

Kubelka–Munk
: a treatment of reflection data that provides an approximate linear relation between signal magnitude and concentration.

overvoltage
: a measure of the departure of an oxidation–reduction system from equilibrium. The corrosion of metal is explicitly a non–equilibrium phenomenon with the overvoltage a measure of the departure from equilibrium. Under non–equilibrium conditions the system is driven towards the state of equilibrium by the overvoltage.

Polarization resistance
: is related to corrosion current density and overvoltage by Ohm's Law. It is used as a measure of metallic corrosion rate.

A area

C concentration

E potential

F Faraday's constant

i, i_{corr} current density

R reflectance

R_p polarization resistance

RT ideal gas constant times absolute temperature

β_a, β_c Tafel constants

γ activity coefficient

η overvoltage

I. Summary and Conclusions.

An effective surface microcell has been developed to determine the effects of humidity, nitrogen dioxide, and nitric acid gases on iron and zinc surfaces. These microcells may be adaptable to field studies of corrosion if studies are conducted to determine a suitable preconditioning of the cell surface or the long term behavior of the cell without conditioning. Such devices provide the inherent advantage of measuring corrosion rate in real-time permitting a meaningful correlation between material damage and the fluctuating pollutant gas concentrations.

Under the conditions employed in this study, the initial effect of exposure to water vapor alone on the materials used in the study (bare carbon-steel, galvanized steel, and painted steel) was very small and negligible in comparison to the effects observed in the presence of an auxiliary corrodant such as NO_2.

No differences were observed in the corrosion process for the two temperatures employed in this study, 10 and 40 C. This would indicate a low energy of activation for the corrosion process. Consequently, the corrosion rate may be diffusion limited, especially at longer exposure times.

The most severe corrosion occurs with exposure to nitrogen dioxide and nitric acid vapor. The metals are markedly altered and the polymeric paint coating to a lesser extent.

Infrared analysis of the surface corrosion products illustrates the nature of the surface alterations. For the pollutants used in this study (NO_2 and HNO_3), ammonium salts were formed which exhibit hygroscopic properties. Hygroscopic salts, which take up water vapor from air, increase the time of wetness of exposed metal surfaces. In the case of the painted steel, the polyester became nitrated on exposure to HNO_3 but was undamaged by exposure to NO_2. The mild damage to the polyester paint by nitric acid may soften the coating lowering its scratch resistance. This, in turn, would promote undercutting by corrosion.

It is important to note that this study was of *initial* corrosion rates which compliment long term corrosion studies, which are recommended for future studies. This data is of use in addressing the important early stages of corrosion. However, as surface coatings weather they develop protective coatings that slow the rate of attack.

The electrochemical and surface spectroscopic methods used in this study have been shown to offer distinct advantages in the study of atmospheric corrosion.

II. Recommendations.

The sensitive methods developed here have immediate application to the study of synergistic interactions such as between nitrogen dioxide and sulfur dioxide.

Nitrogen dioxide is a mild corrodant and may, by itself, exhibit a weak passivating effect on carbon-steel. However, it is suggested that the significance of nitrogen dioxide as an atmospheric corrodant is as a synergist to the corrosive effects of sulfur dioxide.

The effects of sunlight should similarly alter the behavior of exposed iron surfaces as it does for zinc and copper. Like nitrogen dioxide, sunlight should synergistically accelerate corrosion by sulfur dioxide.

Alternate surface wetting occurs with precipitation, fog, and dew events and would dramatically accelerate corrosion and degradation of surface coatings. Accordingly, surface wetting studies should be conducted.

It is therefore recommended that similar studies to these be undertaken using a matrix of humidity, nitrogen dioxide, and sulfur dioxide exposure conditions. The objectives of such studies should be (in order):

- to determine the nature and extent of the synergism between nitrogen dioxide and sulfur dioxide;
- to establish the conditions for extending the use of the surface microcells to field studies;
- to determine the effects of alternate wetting; and
- to determine the effects of sunlight.

III. Introduction.

A. Background.

The deterioration of both natural and man-made materials exposed to the environment is inevitable. Property damage in the United States due to corrosion alone may exceed $70 billion/year for metallic corrosion alone; inclusion of other materials would bring the total cost to over $1 trillion dollars/year![1]

In part, this damage may be attributable to naturally occurring conditions and the nature of the exposed materials. However, since the industrial revolution the increased combustion of fossil fuels has added a burden of acid gases to the atmosphere. These gases, chiefly nitrogenous and sulfurous compounds, may significantly contribute to property damage.

Property damage attributable to pollutant gases constitutes part of the real cost of pollution and is important in determining the cost-to-benefit ratio of pollution control equipment.

The study of atmospheric corrosion of steel by pollutant gases is a relatively new area of study. Traditional methods for investigating atmospheric corrosion involve exposure of material to the ambient atmosphere or to a surrogate salt spray; generally changes in weight (gain or loss) is measured. The purpose of such tests is to estimate the expected life of exposed material rather than to relate cause and effect.

Modern trends in material science are directed towards direct measurements and detailing the processes involved at the molecular level under well characterized and controlled conditions. This is particularly important for atmospheric corrosion where it is necessary to relate cause and effect for economic modeling and given the complexity of the urban atmosphere.

Over 1600 trace gases have been identified in urban[2] air with more than a dozen of these implicated in corrosion processes[3]. Unfortunately, few studies have directly addressed the corrosion of steel by specific pollutant gases such as nitrogen dioxide (NO_2) and nitric acid (HNO_3).

Nitrogen dioxide is not expected to be a major corrosive agent in the atmosphere[3]. In a laboratory study[4], no damage to carbon-steel was observed below 0.5 ppm NO_2. However a strong synergistic effect was observed with sulfur dioxide present and at 50 percent relative humidity (RH). The synergism was not observed at 90 percent RH[5].

The objective of this study is to investigate the potential effect of NO_2 and HNO_3 on carbon-steel, galvanized and painted steel.

B. Methodology.

1. Electrochemical measurements

The conventional methods of corrosion monitoring usually involve measurement of either weight gain due to accumulation of corrosion products or weight loss due to surface dissolution. These methods give only an average measure of corrosion rate over the long time period required for measurable weight change. Furthermore, they are very laborious experimentally and lack sufficient sensitivity to detect the subtle changes which are expected during minor alterations in atmospheric parameters.

Electrochemical polarization methods have been developed in recent years to sensitively measure instantaneous corrosion rate in situ on a continuous basis. These methods are usually confined to corrosion during continuous immersion in a liquid aqueous phase. In the present investigation we have designed and fabricated composite electrode devices to measure corrosion under condensed aqueous surface films.

Polarization methods measure the polarization resistance, R_p, which is the change in potential or overvoltage, η, divided by the change in applied current, i, at low overvoltage. Polarization resistance is related to corrosion current density, i_{corr}, by [6],

$$R_{p=}\frac{\Delta_\eta}{\Delta_i}=\frac{\beta_a\beta_c}{2.3i_{corr}(\beta_a+\beta_C)}$$

where β_a and β_c are the Tafel constants which must be measured from other more extensive electrochemical polarization data. The corrosion current density, i_{corr} is related to the corrosion rate in terms of weight loss per unit area per unit time by Faraday's Law. β_a and β_c both appear in numerator and denominator; thus R_p is relatively insensitive to the exact values of either, and estimates will often suffice for many purposes. In the present investigation, all measured corrosion rates were relatively low, and relative rather than absolute values of corrosion rate are suitable for comparison. Thus, reasonable estimates of these constants were used for substitution in the above equation.

2. Infrared measurements

Surface spectroscopies are finding increasing application in the field of corrosion science. Infrared spectroscopy holds particular appeal due to its ability to provide both quantitative and qualitative information about corrosion processes[7,8,9,10].

Polyatomic material, whether molecular or ionic, possess infrared spectra arising from the vibrational motion of the atoms relative to one another. Because of these vibrational motions the substance can absorb infrared energy at select frequencies determined by inter-atomic distances, atomic masses, and the strength of the inter-atomic attractions. Thus, the infrared spectrum is an intrinsic characteristic of polyatomic molecules and salts. The frequency is generally reported as reciprocal wavelength (cm^{-1}) in the middle infrared region, 4000 – 450 cm^{-1}.

The position of infrared absorption bands relate to the identity of the infrared absorber under analysis. The magnitude of absorption is a measure of the quantity of material interacting with the infrared light. This may be reported as percent transmission, percent reflection, absorption (logarithm of transmittance or logarithm reflection) or in Kubelka–Munk units. The Kubelka–Munk treatment of reflection data provides an ap-

proximate linear relation between reflectance and the quantity of material in the sample. This relation is given by

$$k = \frac{(1-R)^2}{2R}$$

where R is the sample reflectance.

In this study infrared reflection/absorption spectroscopy is applied to the identification of possible corrosion products from the interaction of nitrogenous pollutant gases with metals and an organic coating (paint). Some of these possible products and their approximate group (characteristic) frequencies are given in Table 1.

Table 1. Corrosion Products and Infrared Group Frequencies.

Product	Frequency cm
Nitrite ion	1250
Nitrate ion	1350
Ammonium ion	3200
	1400
Nitrate ester	1650
-COOH	1700

3. Kinetics and thermodynamics

The corrosion of metal and the deterioration of protective coatings can, in large part, be predicted from thermodynamic data. It is important, however, to bear in mind that thermodynamics provide insight only into the equilibrium composition that would result from a reactive mixture. The rate at which that equilibrium state would be achieved is not addressed and is the subject of chemical kinetics. The corrosion of metal is explicitly a non-equilibrium phenomenon with the over-potential a measure of the departure from equilibrium.

At equilibrium the electrode potential is determined from the thermodynamics of the coupled half-cell potentials of the oxidized and reduced forms

$$0 + ne^- \rightarrow R$$

$$R - ne^- \rightarrow O$$

At equilibrium the electrode potential is given by Nernst' Law

$$E_{eq} = E^\circ + \left(\frac{RT}{nF}\right) \ln \frac{C_o}{C_R}$$

where C_O, C_R are the concentrations of the oxidized and reduced forms, T is temperature, R is the ideal gas constant, n is the number of electrons involved in the reaction, E° is the standard oxidation potential and F is Faraday's constant.

Under non–equilibrium conditions the system is driven towards the state of equilibrium by the overpotential, η

$$\eta \equiv E - E_{eq}$$

where E is the electrode potential. The rate at which the reaction proceeds towards equilibrium is related to the flow of electrons in the reaction

$$i_{net} = nFAkC_O^{1-\alpha}\ C_R^{\alpha}[\exp \frac{-\alpha nF\eta}{RT} - \exp \frac{(1-\alpha)nF\eta}{RT}]$$

$$rate = \frac{i_{net}}{nFA}$$

where A is the reacting surface area and α is the cathodic transfer coefficient[10]. This is the Butler–Volmer equation which is equivalent to the Tafel equation:

$$i_{net} = I_{corr}[\exp \frac{\eta}{\beta_c} - \exp -\frac{\eta}{\beta_a}]$$

For a small overpotential rate is proportional to current density and inversely proportional to polarization resistance

$$rate = i_{corr} = \frac{1}{R_p} \times const$$

where the constant and R_p were given earlier. In substituting the transfer coefficients from the Butler–Volmer equation above into the β terms from the Tafel equation, it is seen that the α terms cancel leaving only constants. In actuality, the cathodic transfer coefficient α does not numerically equal the anodic transfer coefficient so that the multiplier of R^{-1}_p is not truly constant but rather a weak function of these parameters.

The corrosion rate may also be determined by direct observation of changes in reactant or product concentrations.

In making kinetic measurements to determine the rate and mechanism of corrosion reactions it is useful to hold all concentrations constant but one and to vary it independently. In this manner the *order dependence* on concentration may be determined. This is the exponent of the concentration term in the rate expression, for example

$$rate = k \times \gamma_{metal} \times P^{a}_{H_2O} \times P^{b}_{NO_2}$$

where γ is the activity of the metal, $\gamma = 1$ by definition, P is the partial pressure of water and nitrogen dioxide with a and b their respective order dependence, and finally k is the rate constant. By fixing all parameters except P_{NO_2}, it is possible to determine the order dependence, b, for NO_2

$$rate = const \times P_{NO_2}^{b}$$

$$\log(rate) = b \times \log(P_{NO_2}) + \log(const).$$

In this way it is possible to determine if the corrosion rate will increase with the square of NO_2 partial pressure (b=2) or linearly (b=1) or exhibit some other dependence. A log–log plot of *relative rate* (*unit–less*) versus *relative NO_2 concentration* (*again, unit–less*) gives the value of b as the slope of the line. This is applicable only to *initial* rate data only.

IV. Experimental Procedures.

A. Materials for study.

Four replicate samples each of the painted, galvanized, and bare steel coupons were exposed in each experiment.

1. Painted and galvanized steel siding

Coated galvanized steel sheet was selected for study because it is commonly used for exterior siding in residential and commercial buildings throughout the United States. Samples were obtained through the courtesy of Marwais Steel Company, Richmond, California. Marwais receives galvanized steel sheet in coil form and applies a paint coating. The painted galvanized steel sheet is then sold to various fabricators.

The coating for this study is typical for siding applications and the sample stock was coated by Marwais in the following manner:

1. Dipped in an alkaline cleaner;
2. Wire brushed;
3. Proprietary amorphous zinc oxide surface applied;
4. Neutralized in a slightly acidic solution of chromic acid;
5. Prime coated on both sides by reverse roll coating to a thickness of 0.2 mils using an epoxy primer with strontium chromate;
6. Cured for 15 to 45 seconds at 400 to 420F;
7. Quenched in water followed by air blowing to dry;
8. Simultaneously roll coated on the front side with a solvent base siliconized polyester topcoat to a thickness of 0.8 mil and on the back side with a non-siliconized polyester backer coat to a thickness of 0.3 mils.; and
9. Cured at 435 to 450F for about 30 sec.

Specimens about 1.5–inch square for FTIR measurements were cut from all samples.

2. Bare galvanized steel

Before the painted sample stock above was coated, a sample from the same coil was taken for comparison in subsequent FTIR measurements. It is notable that the sample

surfaces were not passivated with a chromium solution treatment as is the case with galvanized surfaces normally prepared for atmospheric service. Chromium pretreatments impede adhesion of paint coatings and are specifically prohibited by Marwais specifications.

3. Bare steel

Bare steel samples were produced for FTIR measurements by pickling galvanized coupons in concentrated nitric acid followed by surface abrasion with no. 600 silicon carbide paper to remove remaining traces of zinc.

4. Pure metal foils

Iron, palladium and platinum foil were purchased from AESAR, Johnson Mathey, Inc., Seabrook, NH for fabrication of the electrochemical microcell used for measurement of atmospheric corrosion. The foils were all 0.025 mm thick.

B. Chamber design.

The effect of relative humidity on electrode behavior was first tested in a closed container in which the humidity was controlled by the vapor pressure depression of a saturated salt solution. The series of solutions used and corresponding humidities are listed in Table 2.

Table 2. Saturated Salt Solutions for Humidity Control 760 Torr Atmospheric Pressure. 30°C. Source: ASTM E104.

Saturated Salt Solution	Percent Relative Humidity
$MgCl_2$–H_2O	32
K_2CO_3–$2H_2O$	43
$NaNO_2$	66
NaCl	75
KCl	84
K_2SO_4	97

About 50ml of the appropriate saturated solution was poured into a small 250ml bottle with excess salt to ensure saturation. The bottle was subsequently closed with a rubber stopper with a provision made to hang one of the electrochemical microcells described below in the vapor space above the solution at the bottom of the bottle. The vapor pressure in the enclosed volume above the solution was then allowed to equilibrate for 24 hours with the bottle held in a constant temperature bath controlled at 30°C.

Subsequent measurements used an exposure chamber with continuous flow of reactive gases. This exposure chamber consists of a double walled acrylic box with exterior dimensions of 70 x 33 x 18 cm. There is a gap of about 6mm between the inner and outer walls of the chamber on each side except the top.

Temperature control was effected by flowing thermostatted water through the jacket formed by the double wall. The temperature was set using a Neslab circulating water bath. There are two outlets to the chamber and one common inlet for the recirculating fluid. The inlet is at the bottom edge of the narrow end of the chamber and centered side-to-side. The outlets are at the opposite end and on each side of the top edge.

The flow of reactive gases into the chamber was controlled using an arrangement of needle valves and flow (glass float) measuring tubes (Matheson). Instrument grade air was humidified and mixed with either nitric acid vapors or nitrogen dioxide. The mixing of reactive gases was performed external to the chamber. Humidity was controlled by passing the air through an impinger immersed in distilled water held at a defined temperature for the desired dew point. The air flow was then passed through two traps at the chamber temperature to prevent condensation within the chamber. The humidity of the air in the chamber was then measured optically with a dew point hygrometer (EG&G).

Gas flow through the chamber is by a single inlet and outlet centered in the two end plates of the chamber. At about 6 cm in front of the inlet there is a solid plate partially blocking the chamber. This flow impedance increases turbulent mixing in the chamber. At about 16 cm from the inlet there is a baffle to assure homogeneity of the flow.

Nitrogen dioxide at 90.6 ppm diluted in nitrogen was purchased from Airco and used as delivered. The concentration of nitrogen dioxide in the exposure chamber was checked using a Monitor Labs NOX Analyzer.

Nitric acid vapor above concentrated acid was used as the source of HNO_3 vapor. This gave a "stock" concentration of 250 ppm which was diluted with air to give 1.2 ppm in the chamber. Diluted nitric acid vapors were measured by trapping in distilled water followed by ion chromatographic analysis.

C. Electrodes.

1. Materials and assembly

The electrochemical microcells were of two designs, one to test pure iron foil, the other for the coated galvanized siding product described above. Figure 1 shows the design of the Type A cell used for iron foil. Palladium foil was sandwiched between the iron foil and platinum foil with intervening layers of insulating Mylar polymer film. Electrical contacts were soldered to each foil, and the entire assembly was carefully clamped together and encased in epoxy. The bottom end of the assembly was then carefully ground off to expose the ends of the foil. The iron, palladium, and platinum foils then served as working, reference, and auxiliary electrodes in a microcell exposed to atmospheric conditions. The cell could be renewed after each run by simply abrading the exposed surfaces to expose fresh metal at the ends of the exposed foils.

Type B microcells were similar to Type A but utilized the commercial galvanized and coated siding product as the working electrode in the assembly and allowed exposure of one coated surface. As in Type A, palladium foil was sandwiched between platinum foil and, in this case, the coated steel sheet product, as shown in Figure 2. Again the metal components were insulated with Mylar film, but the epoxy encasement was limited to only one side of the steel sheet, leaving one of the coated surfaces open to the atmosphere.

2. Polarization resistance circuit

Electrical circuitry shown in Figure 3 produced constant controlled levels of DC current and was described in detail previously[11]. A variable voltage (0–30V) filtered DC power supply, PS, provided current through a large variable resistor, R, to the iron working and platinum auxiliary electrodes. R was designed to be very large compared to the cell resistance, r, so that any variations in the latter produced insignificant changes in the total circuit resistance, R + r. Thus, a constant DC voltage from PS across a constant

circuit resistance produced a constant current in the circuit. Current was increased in steps by increasing the voltage output of the power supply, PS.

The potential of the steel or iron working electrode was measured with respect to the unpolarized palladium surface in the microcell, using an electrometer as a null detector in series with a potentiometer. The output from the potentiometer, set to oppose the potential between the working and reference electrodes, gave a measure of the latter when the null detector showed zero potential difference between the two. Any variation from the null caused by an applied current was equal to overvoltage, which could be measured continuously on a strip chart recorder from the output of the electrometer.

3. Calculation of corrosion rates

Corrosion rates were obtained from polarization resistance measurements by procedures previously described[11]. Typical output of the strip chart recorder is shown in Figure 4 during measurements in the closed container with relative humidity controlled at 32 percent with a saturated solution of $MgCl_2$–H_2O. Each current step shows a rapid almost instantaneous increase of potential followed by a slower increase in overvoltage approaching steady state in about 2 minutes at each current step. We interpret the rapid initial increase as ohmic potential generated in the thin film of condensed moisture on the surface. The subsequent slower developing potentials are due to overvoltages caused by the corrosion reactions. Thus, the latter were used to calculate polarization resistance with the ohmic contributions removed.

A simplified measure of polarization resistance was obtained from

$$R_p = \frac{\sum_{n=1,4} \eta_n}{\sum_{n=1,4} I_n}$$

where η_n is the overvoltage at the nth current step I_n. The sum of overvoltages divided by the sum of currents for the first four current levels was used to obtain the polarization resistance. While this value of R_p may be somewhat inaccurate due to non–linearity of overvoltages with current by the 4th current level, the inherent scatter of atmospheric corrosion rates is shown later to be large compared to any such small inaccuracies.

D. FTIR measurement procedures.

The initial instrument used in this study was a Nicolet model 20 SX FTIR. Partway through the study this was upgraded to a Perkin–Elmer model 1800 FTIR with an FR–DTGS detector. The data collected on the Nicolet instrument was transferred to an in–house mainframe computer and translated to the Perkin–Elmer data format with a program written in "C". All the data now reside in the Perkin–Elmer format stored on diskette.

The Perkin–Elmer FTIR is equipped with a variety of computer selectable options to optimize signal–to–noise. These features, such as field stop, mirror velocity, gain, etc., were saved with the spectral data for each spectrum recorded.

The reflection sampling apparatus was purchased from Spectra–Tech. The reflection angle was adjusted for maximum contrast and fixed with a locking screw.

As received, the metal samples exhibited a thin film of surface oil. Accordingly, each sample was cleaned with dishwashing detergent diluted in distilled water, rinsed with

acetone to remove residual water and then dried in air. The back of each sample was then marked by felt-tip pen with the experiment number and a unique sample number. The sample number also served as a marker for sample orientation in the reflection accessory sample holder.

To make an infrared measurement, all the samples were removed from the exposure chamber and the cover of the chamber closed at once. Each sample was placed in the instrument with care to have the same orientation each time and to register the edge of the sample with the edge of the sample mask of the accessory. This assures that the instrument is examining the same spot (about 0.785 cm^2) of the sample each time. All samples were examined and then collectively placed back in the exposure chamber. The total time outside the chamber was about 20 minutes and should be negligible compared to the duration of exposure between measurements (24 to 30 hours).

The infrared spectra were examined for the characteristic group frequencies and saved on diskette. For display purposes the spectra could be examined on a graphics terminal and were transmitted to a second computer equipped with a laser printer for making hardcopy plots of the data. The analysis of the data was based solely on the original numerical form; all hardcopy plots are for illustration only.

E. Exposure conditions.

The investigation of air pollution phenomena in laboratory studies inevitably involve artificial conditions not like those found in the ambient environment. This is part of the price paid to have the controlled and reproducible conditions required to extract kinetic and mechanistic information.

In the ambient atmosphere, humidity may vary from a low of 5 to 10 percent relative humidity (the ratio of absolute humidity, e.g., g m^{-3}, to the maximum value for air saturated with water at the same temperature) to high values in excess of 80 percent relative humidity. There is no typical humidity applicable to laboratory studies. Average humidities are quite varied for different locations and times throughout California. While most laboratory studies use very high humidities (> 90 percent) and long exposure to get sufficient weight change, this study employed more "normal" humidities in the range 20 to 75 percent to better represent those found in the ambient atmosphere. This is possible only due to the sensitivity of the techniques employed to obtain initial rate data.

A major difference between the laboratory and the outdoor exposure is the presence of sunlight. Nitrogen dioxide and metal oxides exhibit photochemical activity in the solar ultraviolet portion of the spectrum of sunlight at the bottom of the troposphere. Nitrogen dioxide photolyzes to produce nitric oxide and the triplet P oxygen atom which rapidly reacts with oxygen to form ozone, a strong oxidizer. In solution, nitrites, and to a lesser extent, nitrates photolyze to produce free radicals including the hydroxyl radical (OH). Some of the OH may combine to form hydrogen peroxide (H_2O_2). Many metal ions, such as ferrous, catalyze a free radical chain decomposition of hydrogen peroxide. Many metal oxides themselves are photochemically active, producing hole-electron pairs. Zinc oxide photolyzed in the presence of liquid water produces hydrogen peroxide in this manner. This is also as aspect of iron (III) oxides in solution. Sunlight was, of course, excluded in this study as it was conducted indoors.

In the ambient atmosphere temperatures vary widely by season. In this study most experiments were conducted at 30°C for convenience. Some measurements were also made for comparison at 5°C and 10°C. In general, corrosion rate is expected to increase with increasing temperature.

The gravest departure from real world conditions occurs with the concentrations of pollutant used. The ambient atmosphere contains over a dozen corrodants, some of which are known to interact synergistically. This study makes no attempt to replicate the atmosphere in this respect. Not only would this constitute an unwieldy matrix of experiments, but the control of concentration levels within natural abundances is not feasible in many instances. Nitrogen dioxide and nitric acid are both reactive and difficult to make reproducibly at low concentrations, moreover at sufficiently low concentrations their effect would be too small to measure directly in a laboratory study. The concentrations used here are greater than those found in the well mixed urban troposphere; this disadvantage is partially offset by determining the reaction order. Only one concentration of nitric acid vapor was used, 1.2 ppm, due to the difficulty in handling this substance. In the urban atmosphere, nitric acid ranges from 0.1 to 10 ppbv (parts per billion by volume). Nitrogen dioxide ranges from about 10 to 100 ppbv in the urban atmosphere. In this study 0.7, 2.5, 5.0, 10.0 and 0 (none added) ppmv (parts per million by volume) nitrogen dioxide was used.

V. Results and Discussion.

A. Effects of humidity.

All samples were exposed for a minimum of 120 hours for all conditions employed in the study with the exception of the nitric acid exposure experiment. Due to the rapid and severe damage induced by HNO_3, the exposure was stopped at 30 hours. Under these conditions, integrated exposure doses of 0 to 1200 ppm–hours were used for NO_2 and 36 ppm–hours for HNO_3. This compares to annual average exposures of 205 to 473 ppm–hours for NO_2 in the South Coast Air Basin[14] in 1985 and to an average exposure of 24 ppm–hours of HNO_3 observed at Claremont in 1985[13]. Figure 5 shows the humidity dependence of polarization resistance for the iron foil specimens in the Type A microcell. Iron shows a reasonably strong dependence of corrosion on humidity. The polarization resistance decreases (corrosion rate increases) as humidity increases to about 60 percent, above which the values level off, presumably because of surface full saturation or coverage by the surface moisture film.

Results from electrochemical measurements on painted galvanized steel specimens in the Type B microcell (Figure 2) are shown in Figure 6. The polarization resistance values, which are inversely proportional to corrosion rate, showed only a weak dependence on humidity up to about 75 percent, above which the corrosion rate increased rapidly. However, the corrosion rates for the galvanized specimens are several orders of magnitude higher than for the uncoated iron specimens. For the galvanized specimens, a galvanic couple exists between the zinc coating and the adjoining steel substrate. The galvanic current is rather high and concentrated at the small surface area of zinc at the exposed edge of the coated specimen. Polarization resistance in this case measures the galvanic current passing between the two metals and is consequently low compared to the values for iron in Figure 5.

There was no evidence of degradation of the paint coating or undercutting of the coating in these short tests. Much longer testing times would be necessary to demonstrate attack on or under the painted coating. Nevertheless, these tests demonstrate the utility of the microcell configuration. Further testing at longer times and in alternate immersion conditions[12] would show the usefulness of the Type B configuration for paint testing and evaluation.

These brief exposures gave little or no deterioration of the metal or coated surfaces detectable by infrared reflection–absorption spectroscopy.

Figure 7 shows the effect on painted steel of exposure to 17.5 mg/l water at 31°C. This corresponds to 53.6 percent relative humidity. The ester band (1740 cm^{-1}) and to a lesser extent the acid band (1700 cm^{-1}) is reduced in intensity with exposure. Within the accuracy of the data, the polymer is not appreciably degraded by exposure to moist air.

Figure 8 shows the effect of humidity on zinc (3500 cm^{-1}) (galvanized steel) under the same conditions. In generating this figure, the extinction at 3500 cm^{-1} on the metal surface was used as a measure of damage. It is reasoned that even for slight corrosion the porous corrosion layer will hold moisture which will contribute to extinction in this region. Hence, this figure also includes the accumulation of moisture resulting from surface changes. Again, within the accuracy of the data, no deterioration of the surface is detected by reflection spectroscopy.

Figure 9 shows the effect of humidity on bare carbon steel. In generating this figure the extinction at 3500 cm^{-1} on the metal surface was used as a measure of damage. Hence, this figure also includes the accumulation of moisture resulting from surface changes. Within the accuracy of the reflectance data, there is little observable effect for these short exposures. The damage is small compared to that which occurs in the presence of an auxiliary corrodant such as nitrogen dioxide or nitric acid as will be seen in the following sections.

B. Effects of nitrogen dioxide.

At the highest level of nitrogen dioxide used (10 ppmv), no damage to the painted steel was observed using infrared spectroscopy over the course of exposure. Figure 10 shows a slight reduction in the carbonyl frequencies (ester band at 1740 cm^{-1}) essentially like that observed in the absence of nitrogen dioxide. Within the scatter of the data there is no observed degradation of the paint by the nitrogen dioxide.

Exposure of bare steel to 10 ppmv nitrogen dioxide did produce corrosion as evident by the decreased reflectance in the 3500 cm^{-1} region. This is shown in Figure 11. The reflectance spectra before and after exposure to nitrogen dioxide at 10 ppmv are shown in Figure 12. A weak band due to nitrate is observed at 1360 cm^{-1}.

Exposure of zinc (galvanized steel) to 10 ppmv nitrogen dioxide results in the formation of surface nitrate as evidenced by appearance of an absorption band in the nitrate frequency region (1350 cm^{-1}). There is weak extinction in the ammonium ion regions (3200 cm^{-1} and 1400 cm^{-1}) as well (Figure 13). The accumulation of nitrate on the surface with time of exposure is shown in Figure 14. At earlier exposures ammonium ion is also detected as a product as seen in Figure 15. In this figure the ammonium ion absorption bands are quite pronounced (3200 cm^{-1} and 1400 cm^{-1}).

Figure 16 shows the effect of NO_2 on the uncoated pure iron in the Type A microcell. Polarization resistance increased from relatively low levels without NO_2 to values an order of magnitude higher when NO_2 was increased to 5 ppm in an atmosphere containing 65 percent humidity. This indicates that NO_2 has an inhibiting effect on the corrosion of iron.

Polarization resistance shows a tendency to also increase with increasing NO_2 for the galvanized specimen in the Type B microcell (Figure 17). However, the tendency is weak, and the increase could be within the possible scatter of data. In both Figure 16 and 17, the polarization resistance is somewhat lower in the continuous flow chamber as compared to the static chamber (see Figures 5 and 6). The increase only brings the polari-

zation resistance up to the level shown in Figure 5 for the humid atmosphere at 65 percent humidity without NO_2.

The electrochemical data shown in Figure 16 indicates the initial corrosion rate is near linear in nitrogen dioxide concentration. This is in agreement with the order dependence from the infrared data as shown in Figure 18. The points plotted in Figure 18 correspond to 0.7, 5, and 10 ppm nitrogen dioxide. The approximately unit slope indicates a linear dependence of corrosion rate on NO_2 concentration.

C. Effects of nitric acid.

Measurement of polarization resistance (R_p) using the type A cell assembly in the presence of nitric acid vapor was unsuccessful. After introducing a nitric acid concentration of 1.2 ppm in the exposure chamber, the polarization resistance was too small to measure with our instrumentation. Attempts to make measurements at lower nitric acid concentrations by exponential dilution of the exposure chamber were also unsuccessful.

Under the test conditions of 65 percent relative humidity at 30°C, the ohmic component of resistance comprised virtually all the response from the applied excitation current (the order of picoamps). The characteristic polarization curve (see Figure 4) was not observed. Adjustments in the relative humidity was also unsuccessful in increasing the polarization component of resistance.

It is assumed that nitric acid is sufficiently corrosive to iron that the R_p is reduced below our detection capability in the presence of high ohmic resistance in a tarnish film even at nitric acid concentrations below 1 ppm. With the use of permeation devices and precision mass flow controllers it should be possible to reproducibly generate acid concentrations in the 100 ppb range. Polarization resistance measurements might be feasible under these conditions.

The effects of nitric acid (HNO_3) fumes on painted, galvanized, and bare carbon-steel were investigated using reflectance infrared spectroscopy. Infrared techniques compliment the electrochemical methods in that rates too fast for the electrochemical technique may fall in the range of the infrared method and conversely the rates that are too small to produce measurable corrosion by the infrared technique are addressable with the electrochemical cells.

Sample coupons and the surface microelectrode assembly were exposed to 1.2 ppm HNO_3 in the exposure chamber. The damage was severe and rapid. The surface electrode assembly could not record corrosion at rates as high as those encountered. The damage in the first few hours was also sufficient to hamper the infrared reflection-absorption measurements.

Because the damage was so severe and rapid, the exposures were halted at 30 hours to achieve initial exposure conditions. This corresponds to an integrated dosage of 36 ppm-hours. By comparison, ambient nitric acid concentration averaged 0.51 ppm-hours over a nine day sampling period at Claremont in a field study. This rate of exposure would be equivalent to the yearly dosage of 24 ppm-hours of HNO_3.[13].

The aggressive nature of the HNO_3 corrosion was too severe to obtain reasonable estimates of reaction rate, however, corrosion products arising from the reaction were identifiable.

Figure 19 is the reflection-absorption infrared spectrum of the corrosion products formed from HNO_3 - zinc (galvanized steel) interaction. The initial or before exposure spectrum corresponds to the right side scale. Zinc nitrate is the principal product (1350 cm^{-1} region). Nitrite (1250 cm^{-1} region) and ammonium ion signatures (3200 cm^{-1} and

1400 cm^{-1} regions) are also observable in the R–A spectra of the exposed galvanized steel coupons (Figure 20).

Iron nitrate (1360 cm^{-1}) appears to be the principal product (aside from hydroxy iron oxides) from exposure of bare carbon–steel to 1.2 ppm HNO_3 gas (Figure 21).

The least damage occurred with the painted coupons. After 30 hours exposure to 1.2 ppm HNO_3, there was no visible damage to the coupons. However, infrared reflection–absorption spectra of the painted surface revealed a slight loss of the organic ester component (1740 cm^{-1} region) and the formation of nitrate ester (1650 cm^{-1} region, Figures 22 and 23).

D. Effects of temperature.

The effects of temperature were investigated from 10°C to 40°C with nitrogen dioxide held constant at 2.5 ppm and the *absolute* humidity held at 0.0063 grams of water vapor per liter of air. This corresponds to approximately 71 percent relative humidity (at 10°C) to 12 percent relative humidity (at 40°C).

Within the accuracy of the data, there was no observed effect of temperature in this range indicating a low energy of activation for the corrosion process.

References

1. Baer, D.R. and M.T. Thomas, 1982,
   Industrial Applications of Surface Analysis, ACS Symposium Series 199, L.A. Casper and C.J. Powell, eds., American Chemical Society, Wash. DC

2. Graedel, T.E., 1978,
   Chemical Compounds in the Atmosphere, Academic Press, NY.

3. Graedel, T.E., 1984,
   9th International Congress on Metallic Corrosion, Toronto, Can., June 3–7.

4. Johansson, L.G., 1985,
   Electrochemical Society Fall Meeting, Las Vegas, NV, Oct.

5. Johansson, L.G., 1984,
   9th International Congress on Metallic Corrosion, Toronto, Can., June 3–7.

6. Stern, M. and A.L. Geary, 1957,
   A Theoretical Analysis of the Shape of Polarization Curves, J. Electrochem. Soc., 104, 56.

7. J.M. Aceves, I.D. Couper, and M.A. Sanchez, 1982,
   IEEE International Symp. Electrical Insulation, 229–232.

8. T. Nguyen and W.E. Byrd, 1985,
   Reflection/Absorption Fourier Transform Infrared Spectroscopy Studies of the Degradation of Organic Protective Coatings on Steel, American Chemical Society Symposium on Polymeric Materials, Chicago, Ill.

9. A.E. Dowrey and C. Marcott, 1982,
   A Double–Modulation Fourier Transform Infrared Approach to Studying Adsorbates on Metal Surfaces, Applied Spectroscopy, 36, 414–416.

10. P.T. Kissinger and W.R. Heineman, 1984,
    Laboratory Techniques in Electroanalytical Chemistry, Marcel Dekker, Inc., NY.

11. Jones, D.A., 1983,
    The Advantages of Galvanostatic Polarization Resistance Measurements, Corrosion, 39, 444–448.

12. Jones, D.A., R.K. Blitz, and I. Hodjati, 1986,
    Alternate Immersion Testing of Coated Sheet Steel, Corrosion, 42, 255.

13. Private communication from Manjit Ahuja, California Air Resources Board, cited from Hering, S.V., et al, 1987,
    The Nitric Acid Shootout: Field Comparison of Measurement Methods in press.

14. Private communication from Manjit Ahuja, California Air Resources Board, cited from *California Air Quality Data 1985*, California Air Resources Board.

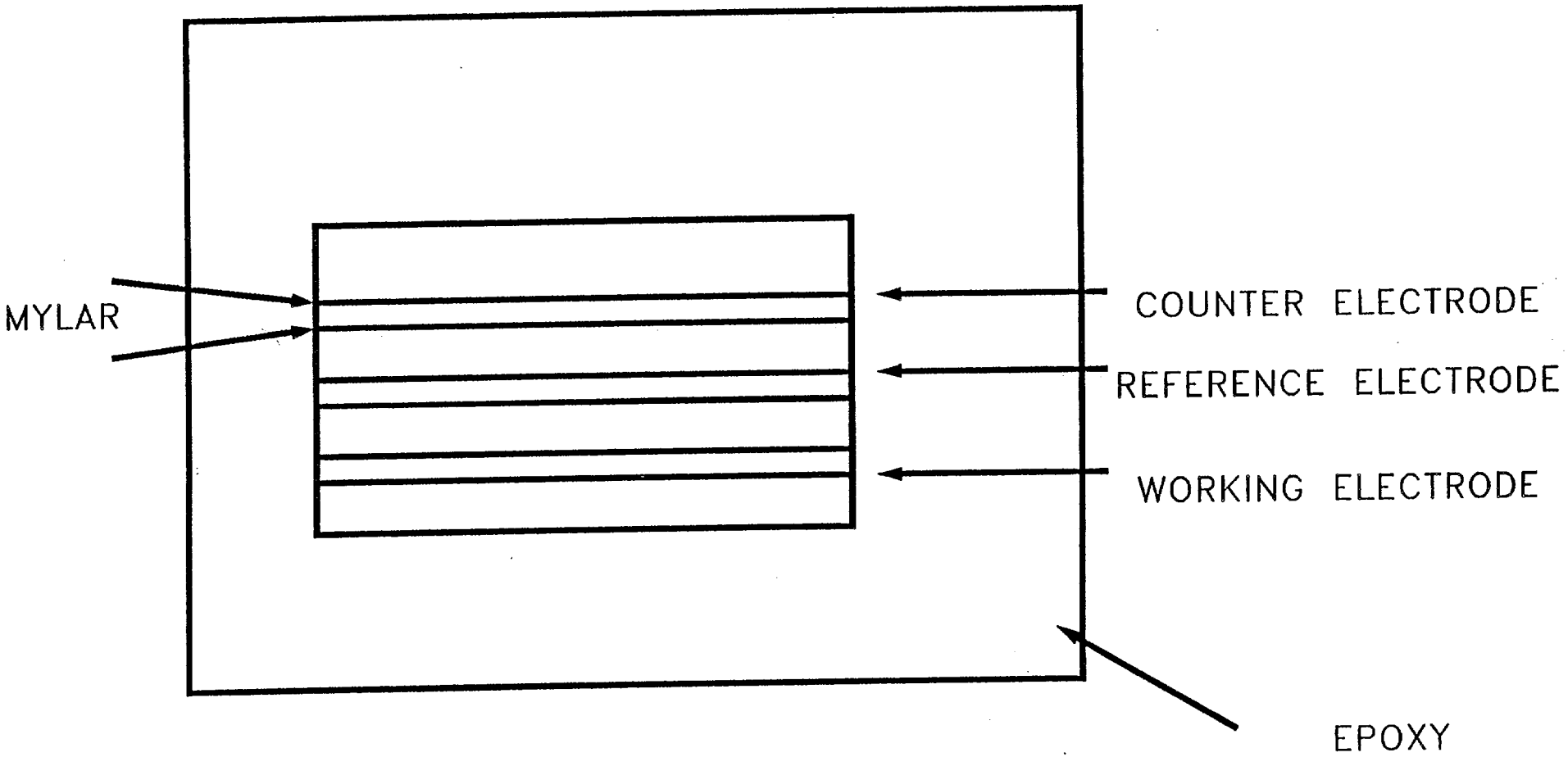

Figure 1. Surface electrochemical cell type A.

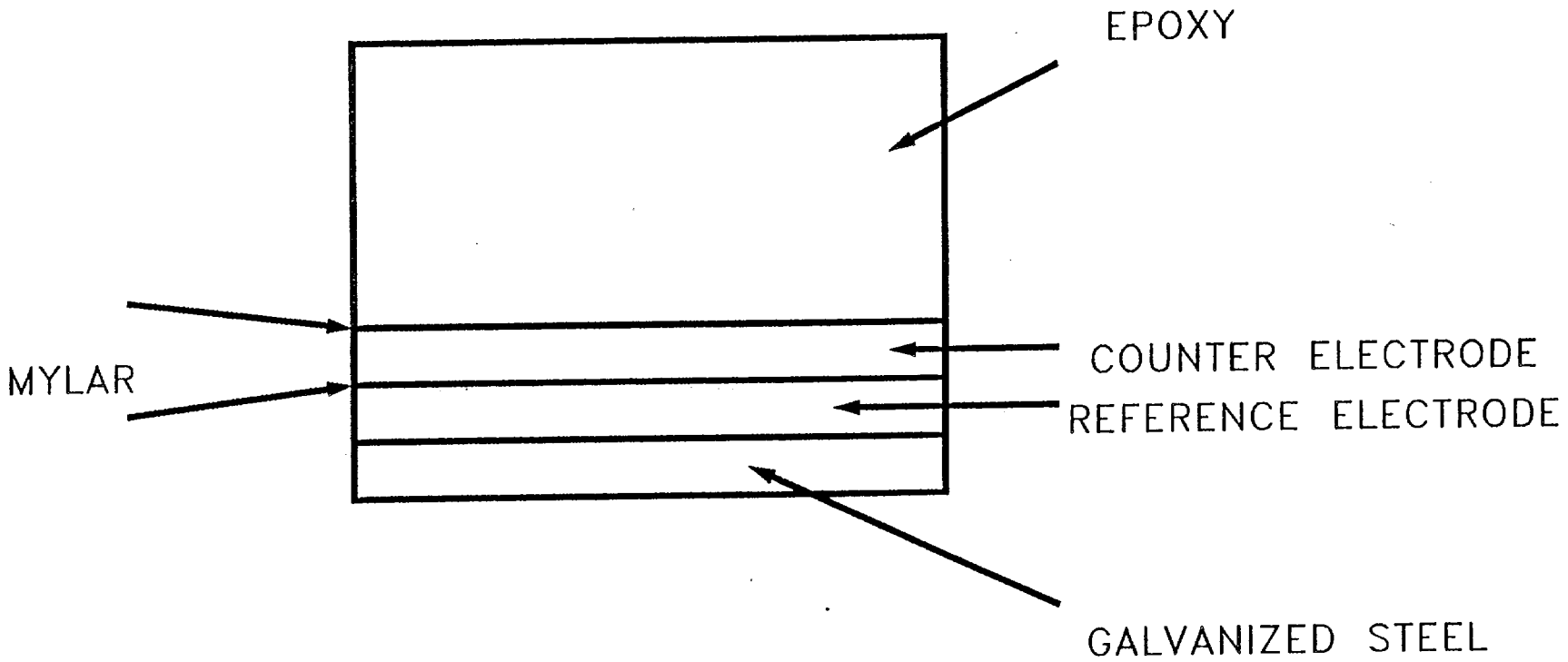

Figure 2. Surface electrochemical cell type B.

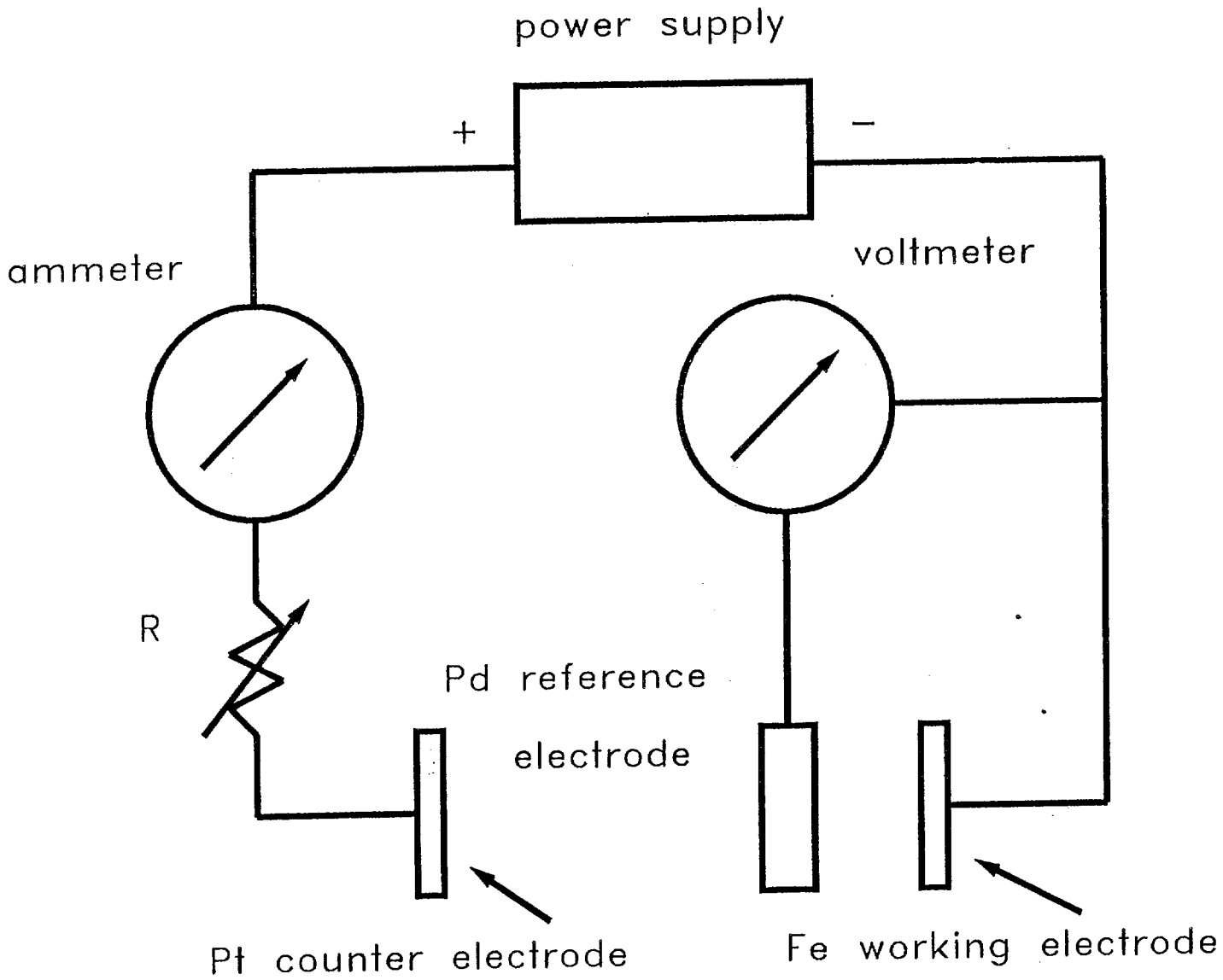

Figure 3. Polarization resistance circuit.

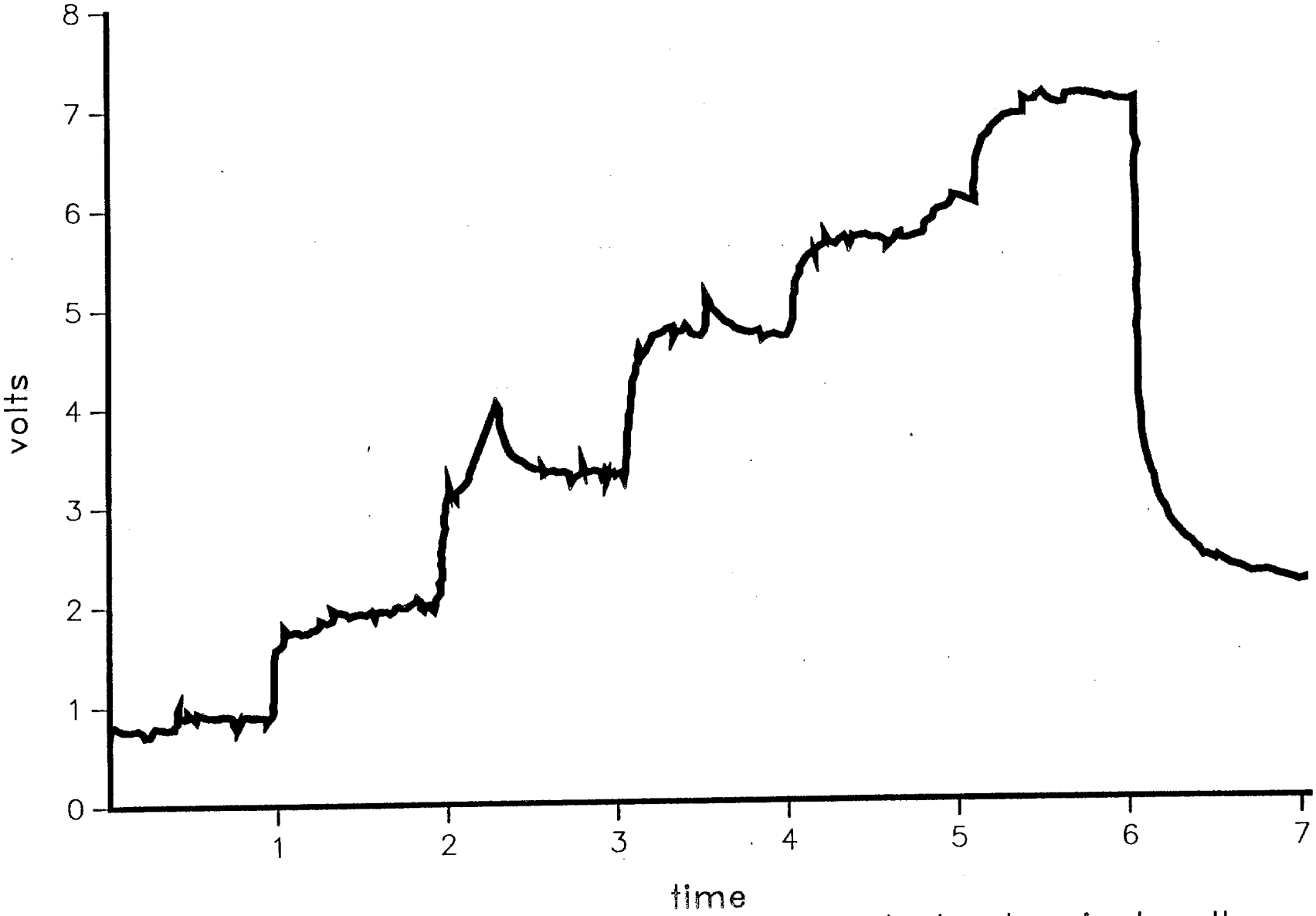

Figure 4. Typical response of surface electrochemical cell.

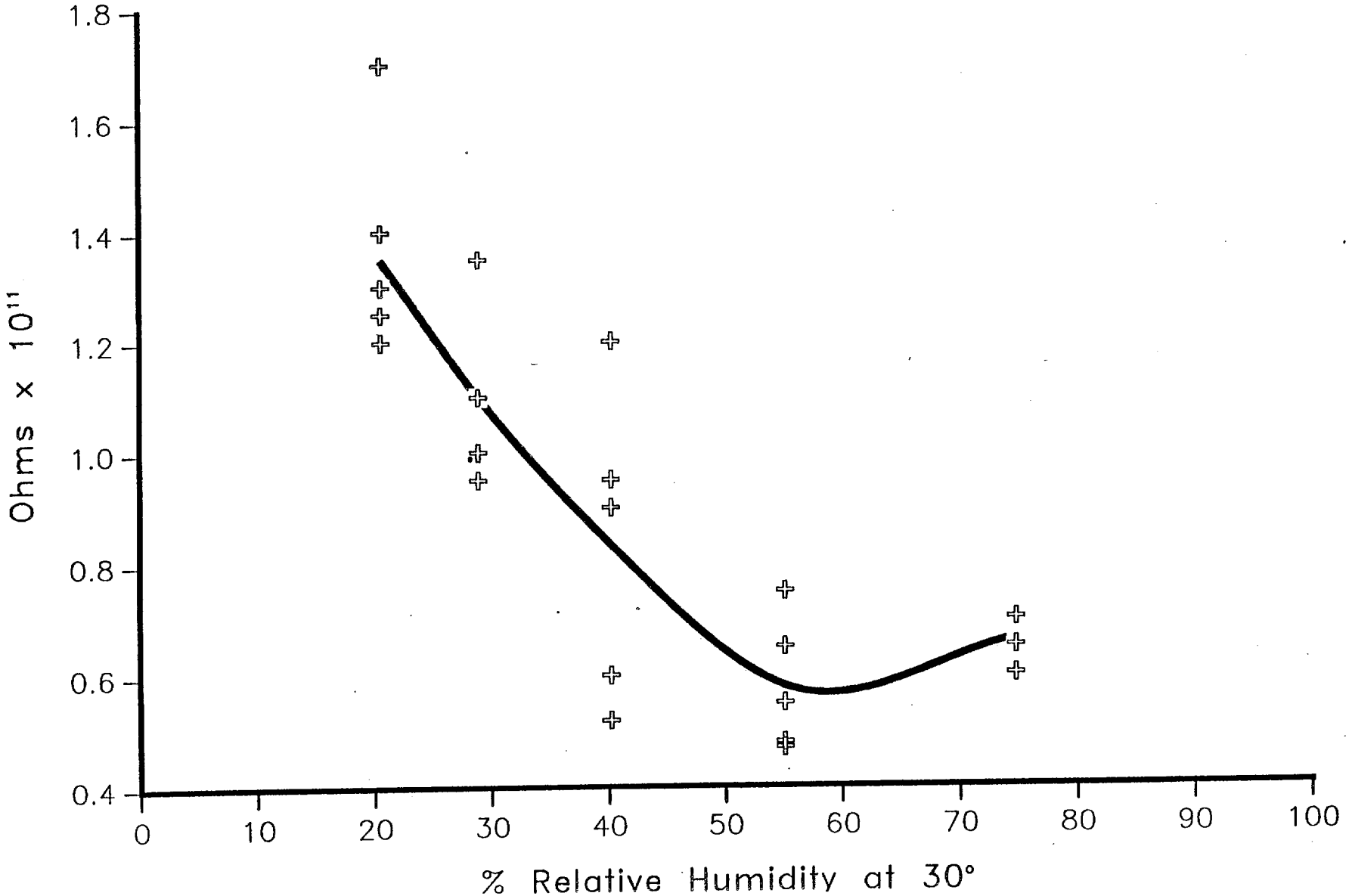

Figure 5. Type A cell response to humidity.

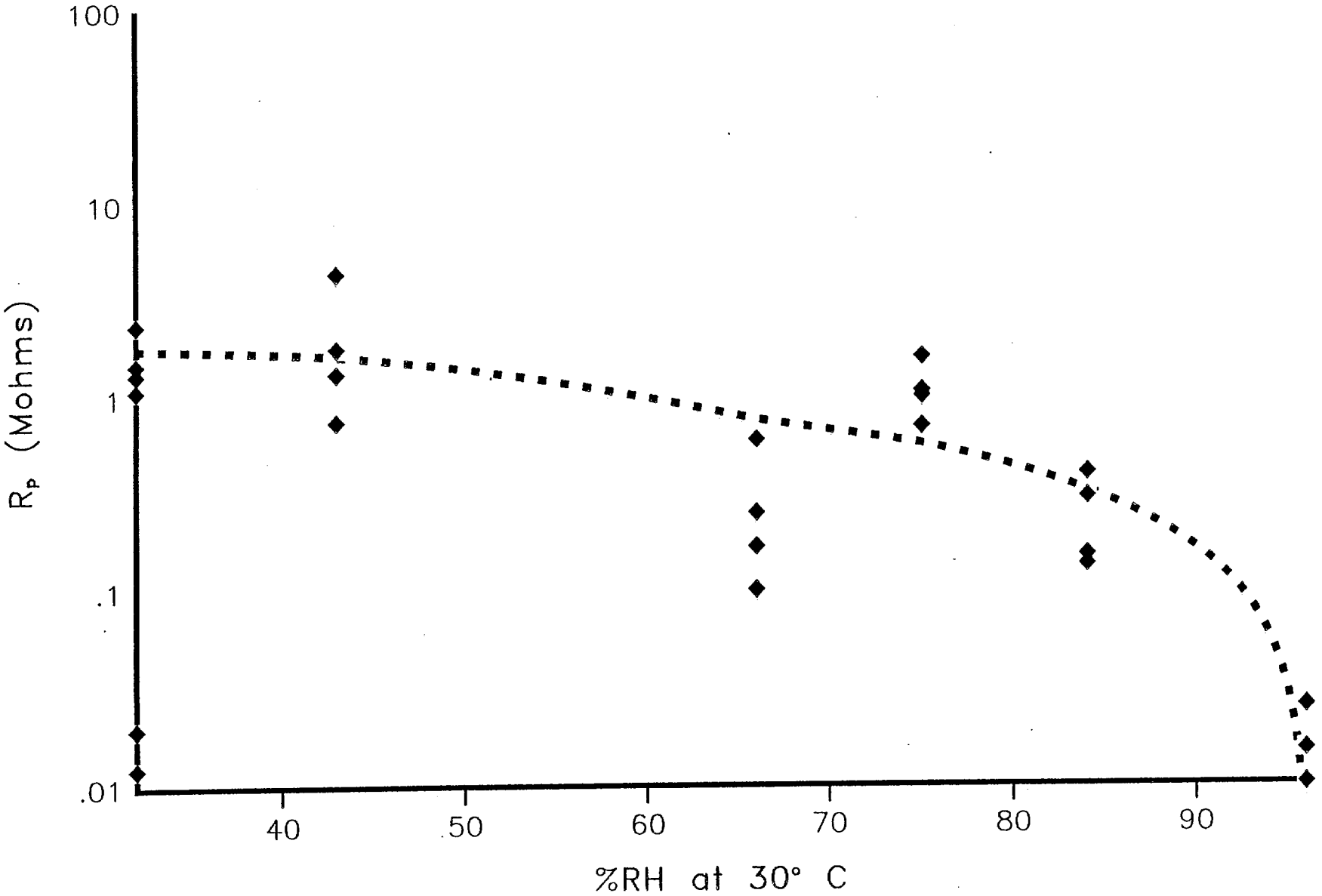

Figure 6. Type B cell response to humidity.

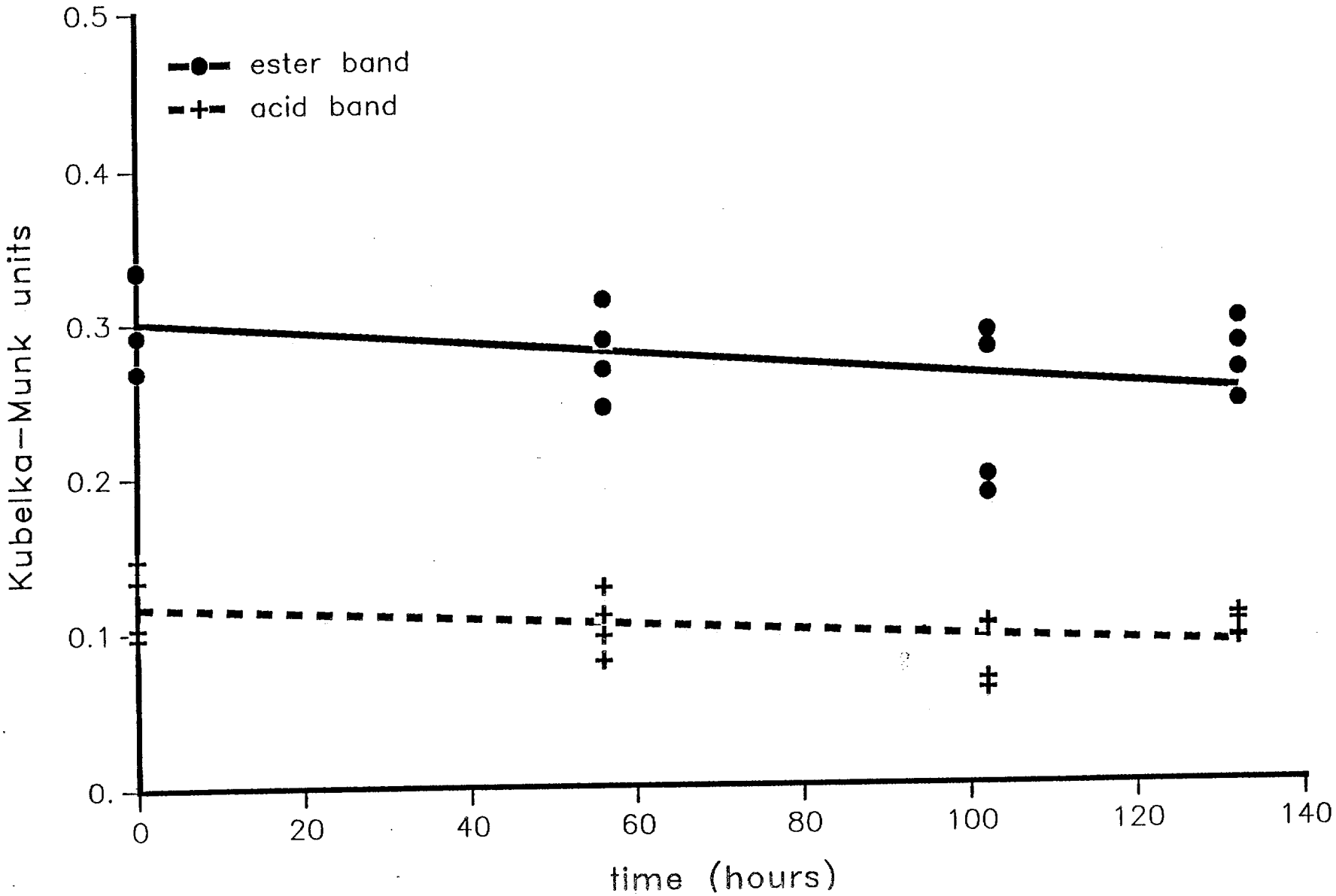

Figure 7. Effect of humidity on painted steel.

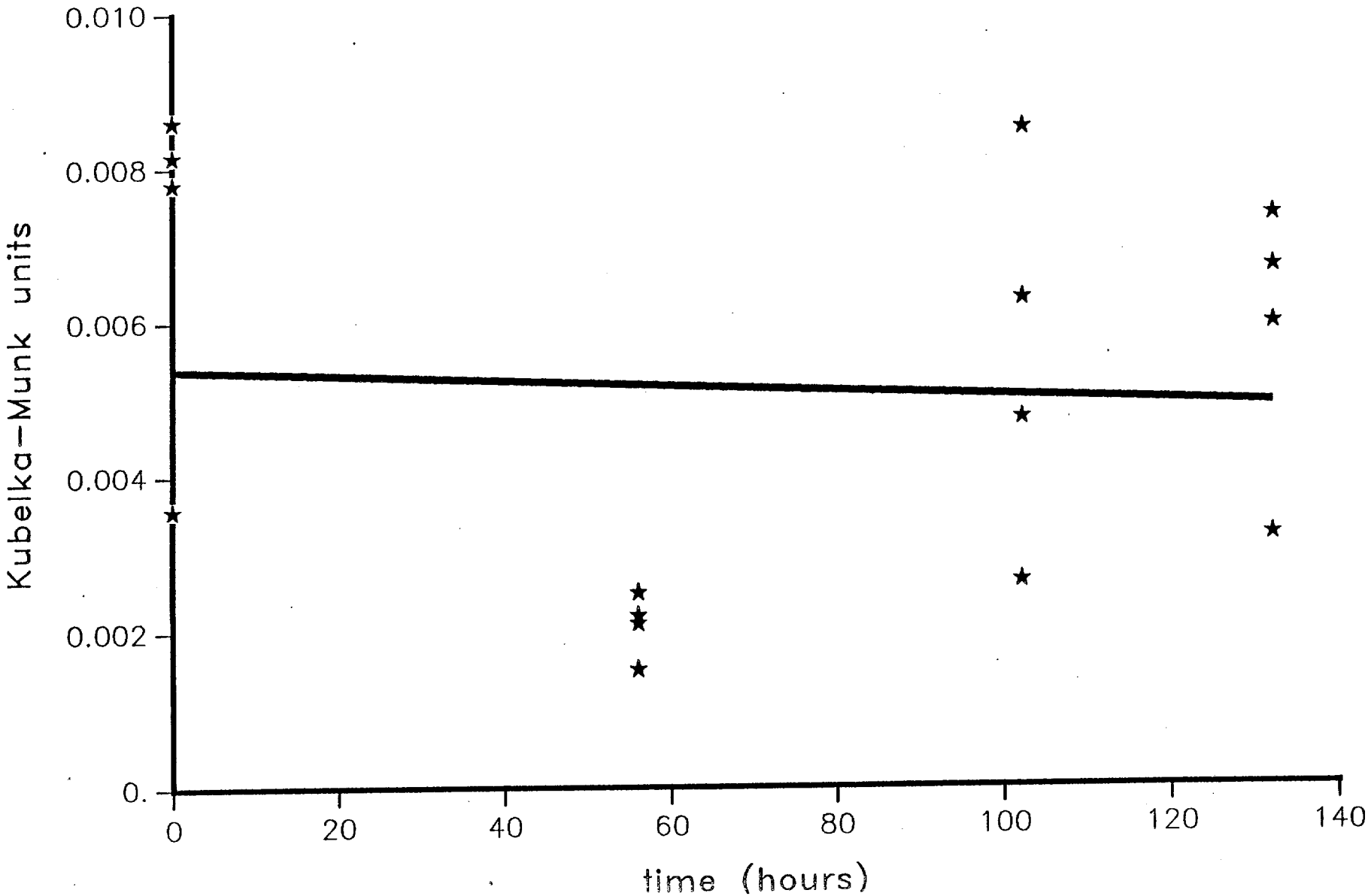

Figure 8. Effect of humidity on galvanized steel.

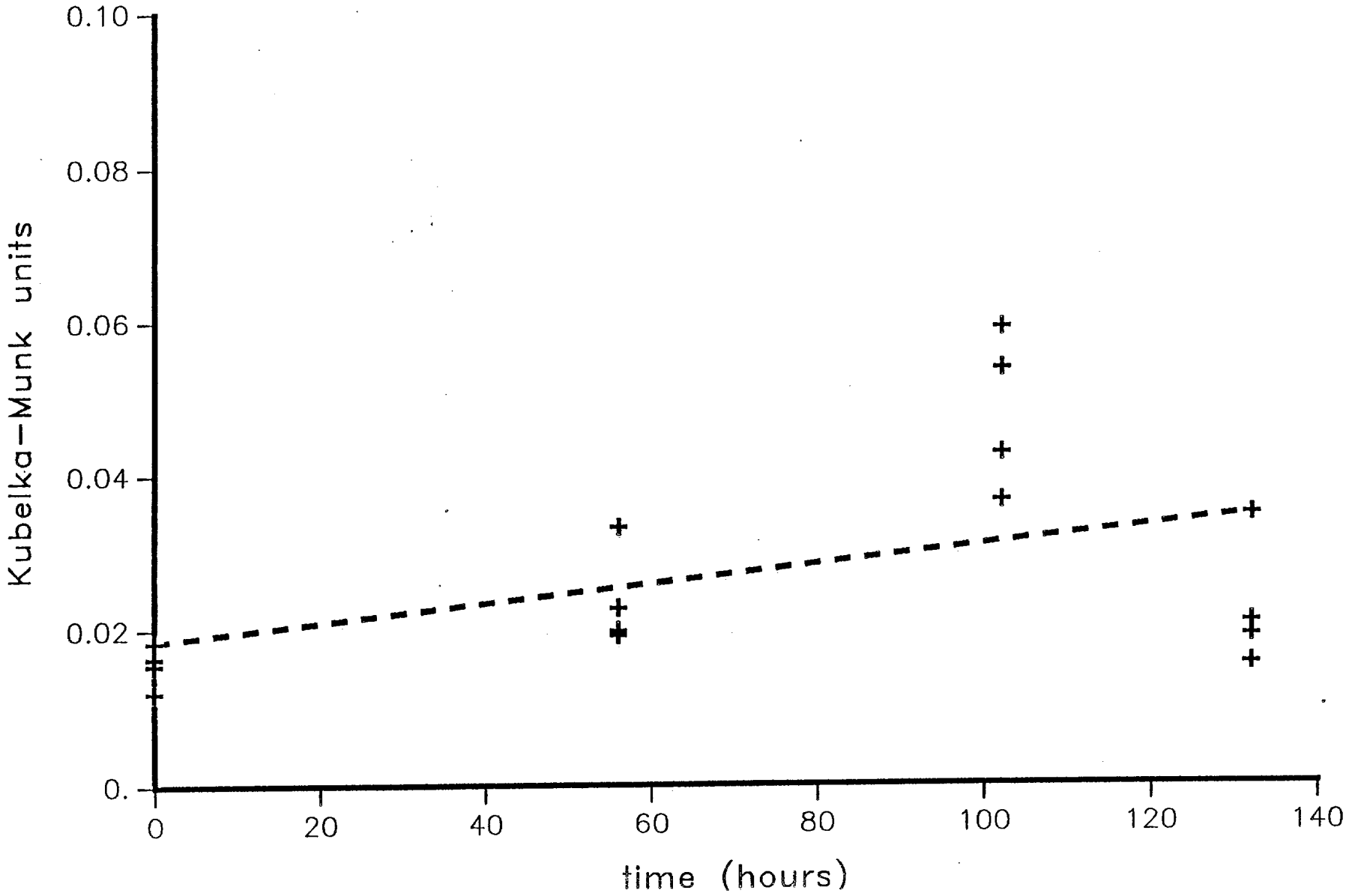

Figure 9. Effect of humidity on bare steel.

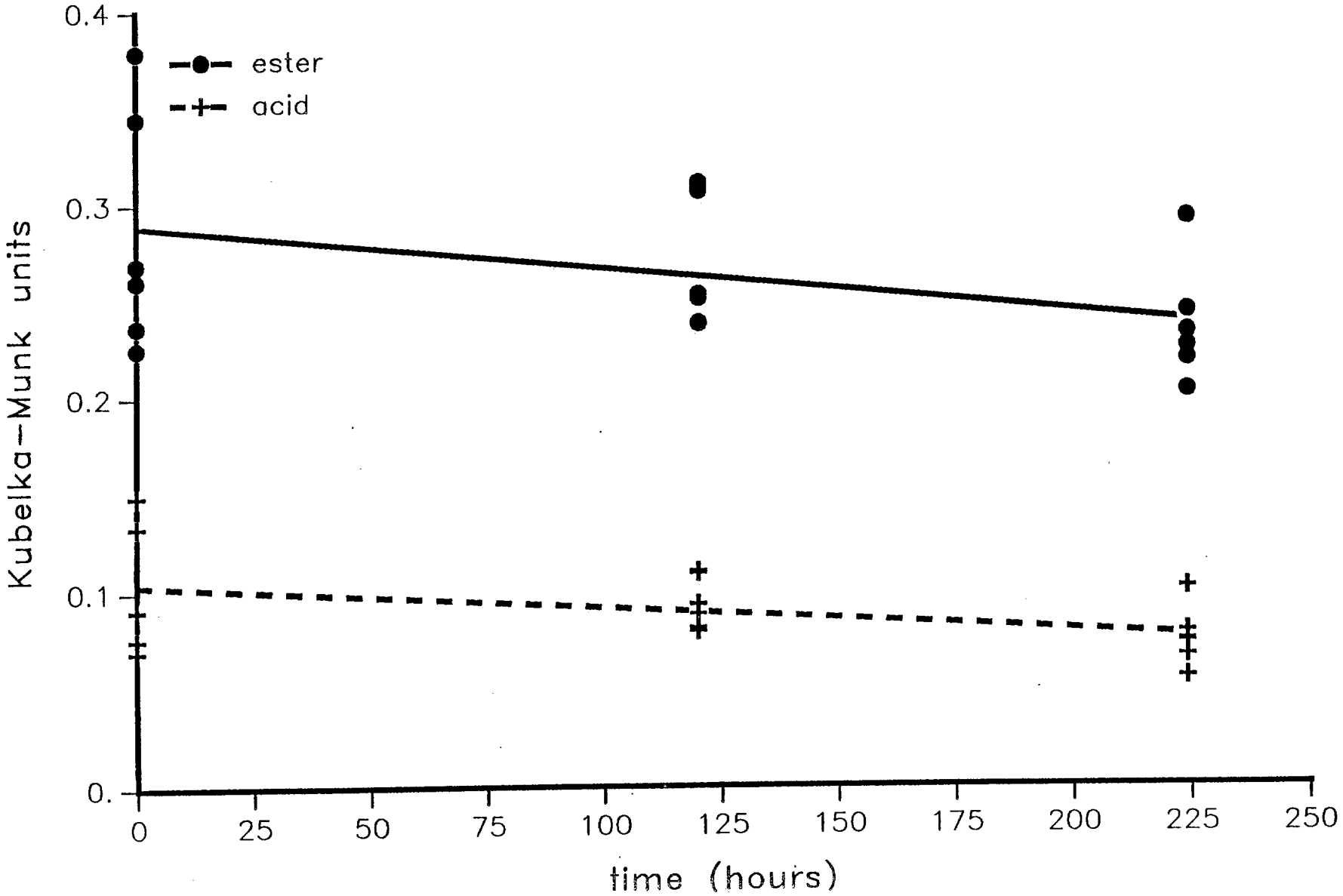

Figure 10. Effect of 10ppm NO_2 on painted steel.

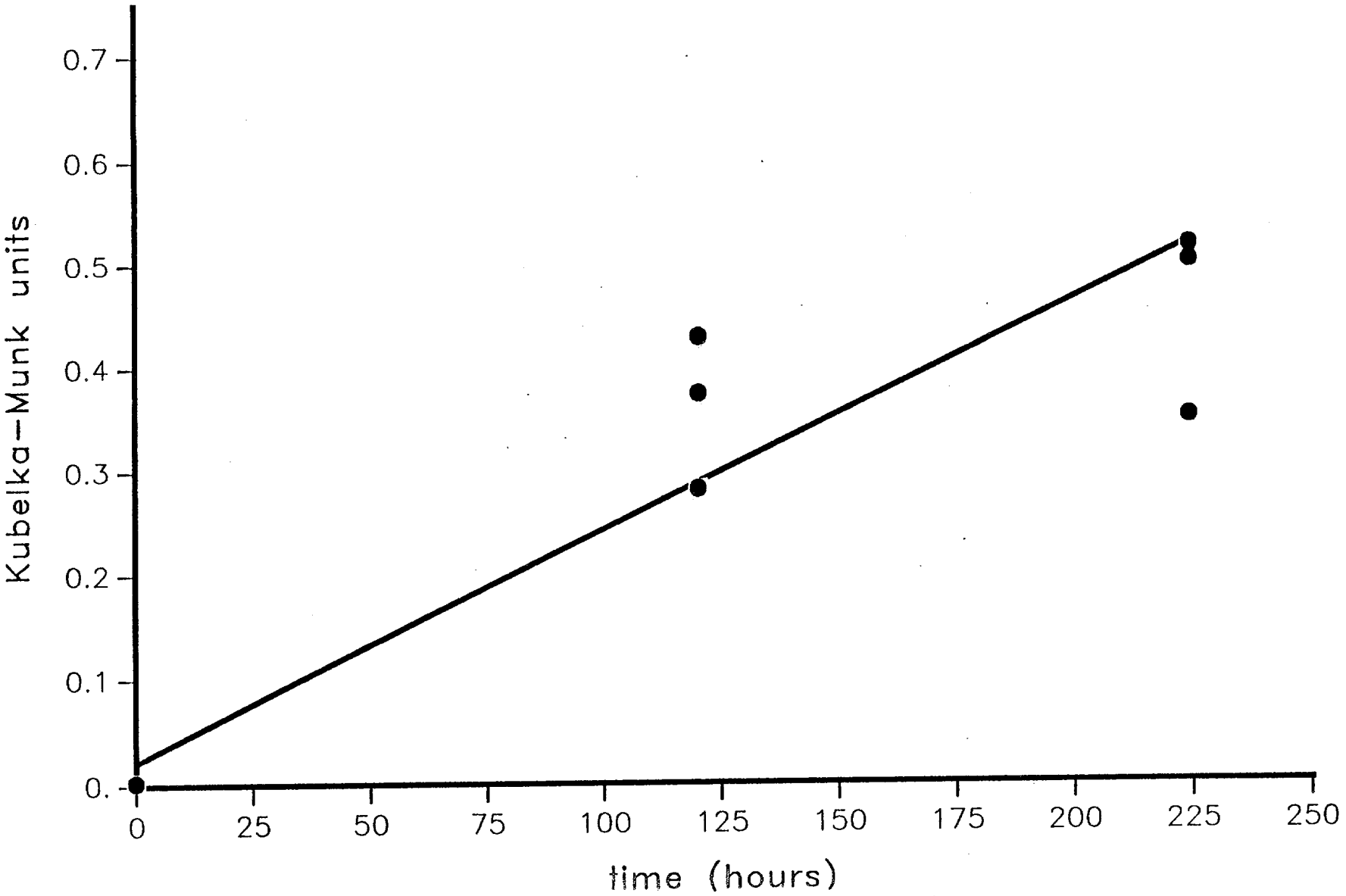

Figure 11. Effect of 10ppm NO_2 on bare steel.

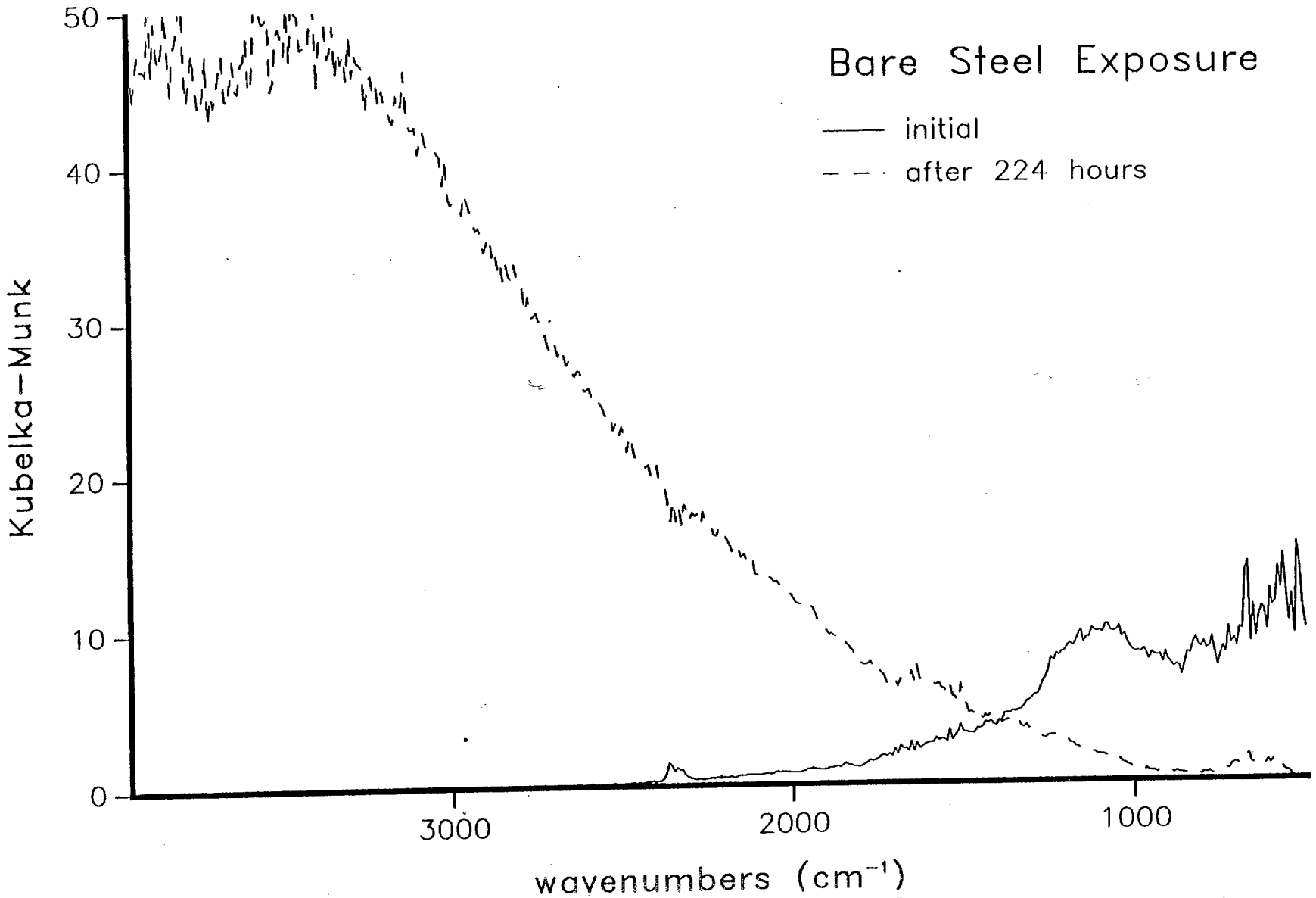

Figure 12. Reaction of steel with 10ppm NO_2.

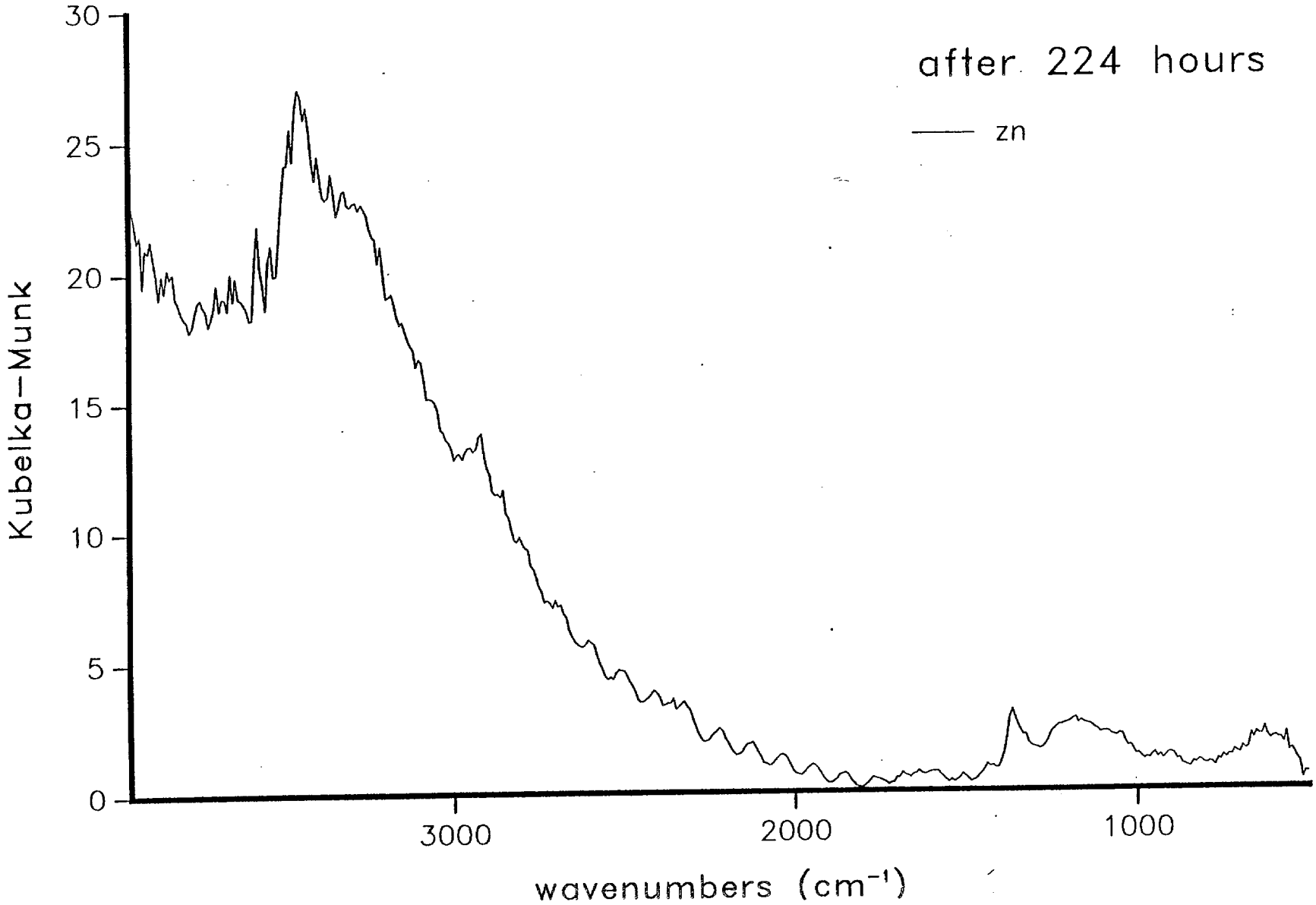

Figure 13. Effect of NO_2 on zinc at long time.

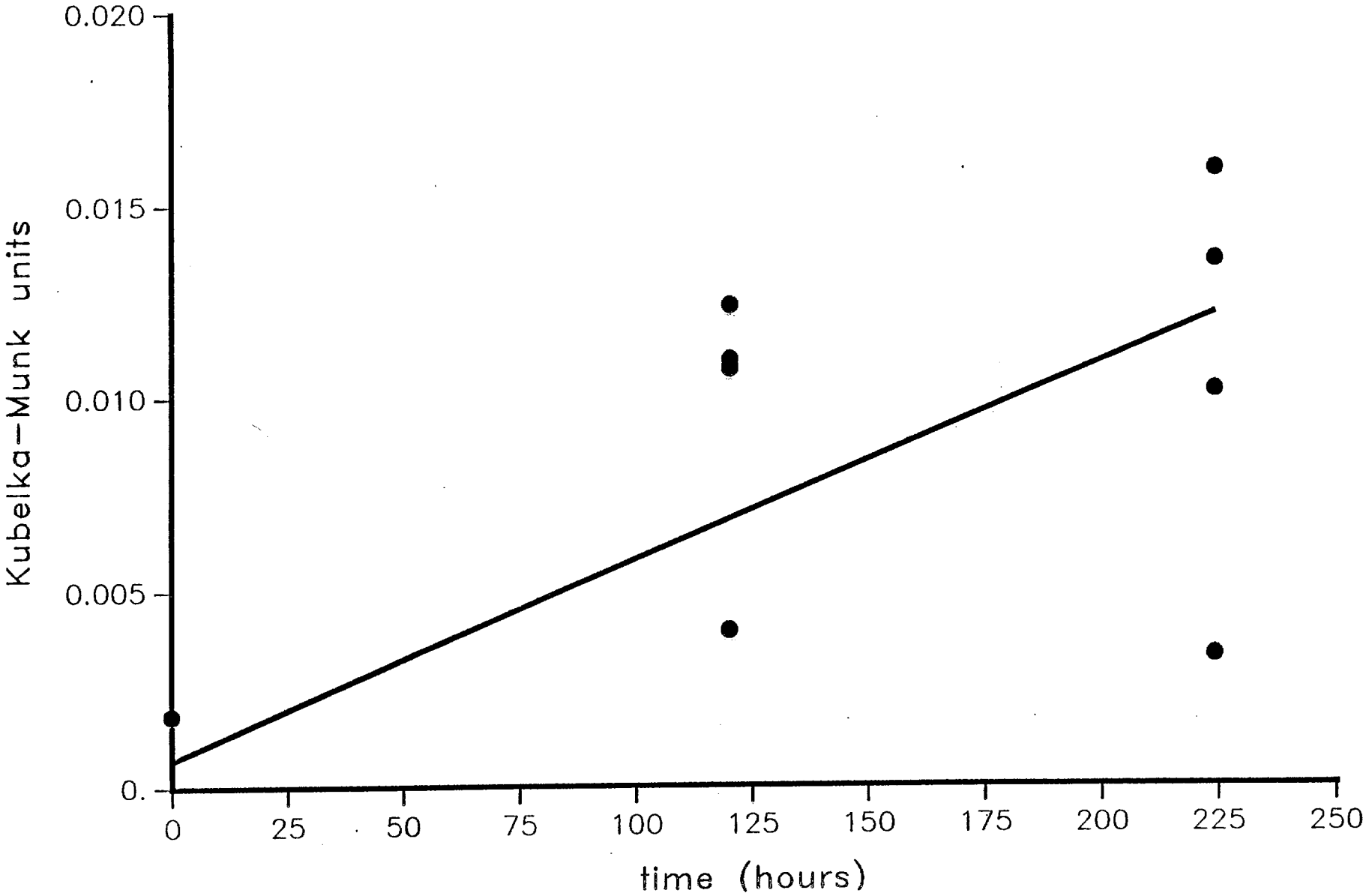

Figure 14. Effect of 10ppm NO_2 on zinc.

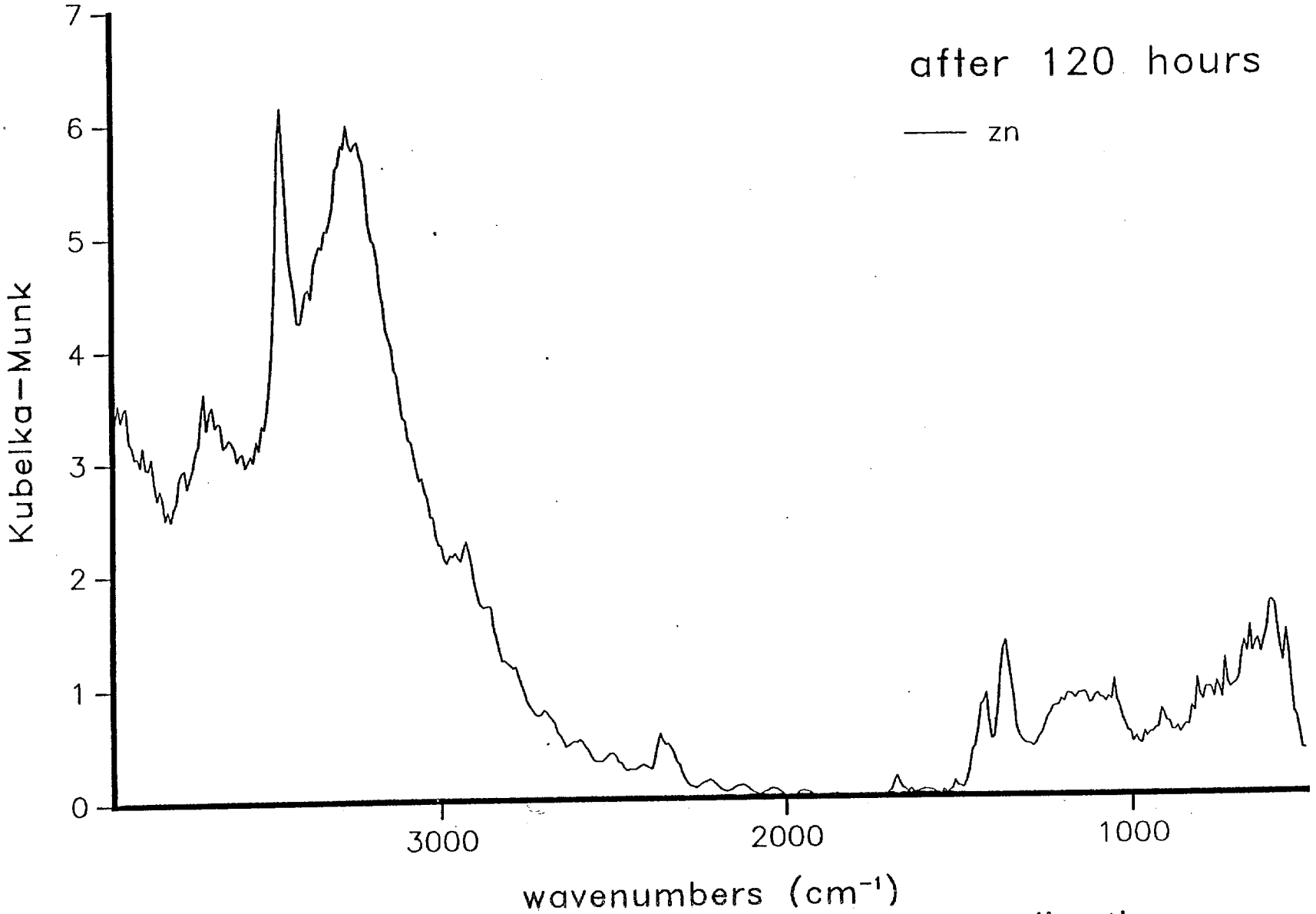

Figure 15. Same sample as in Figure 14 but at earlier time.

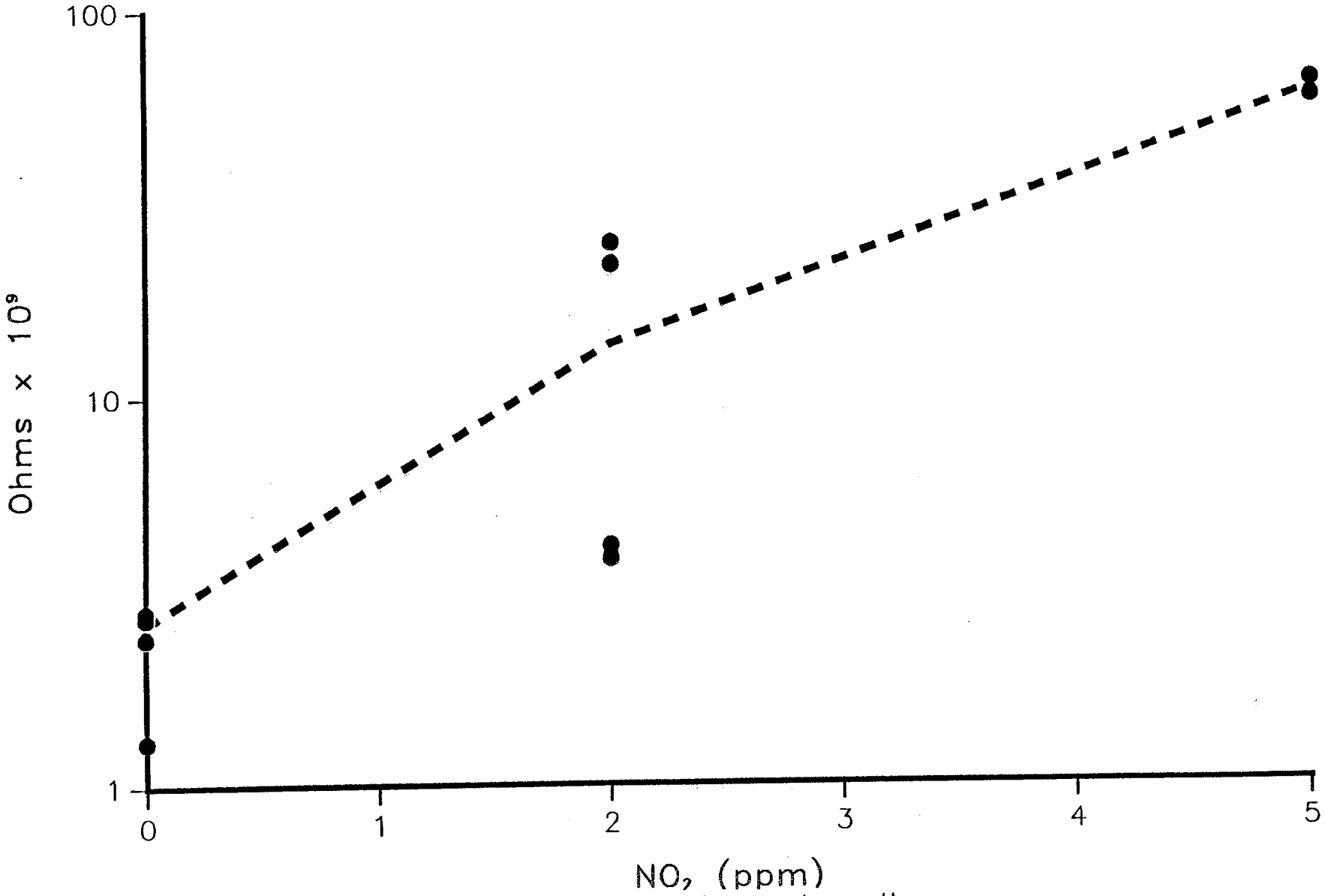

Figure 16. Effect of NO_2 on type A cell.

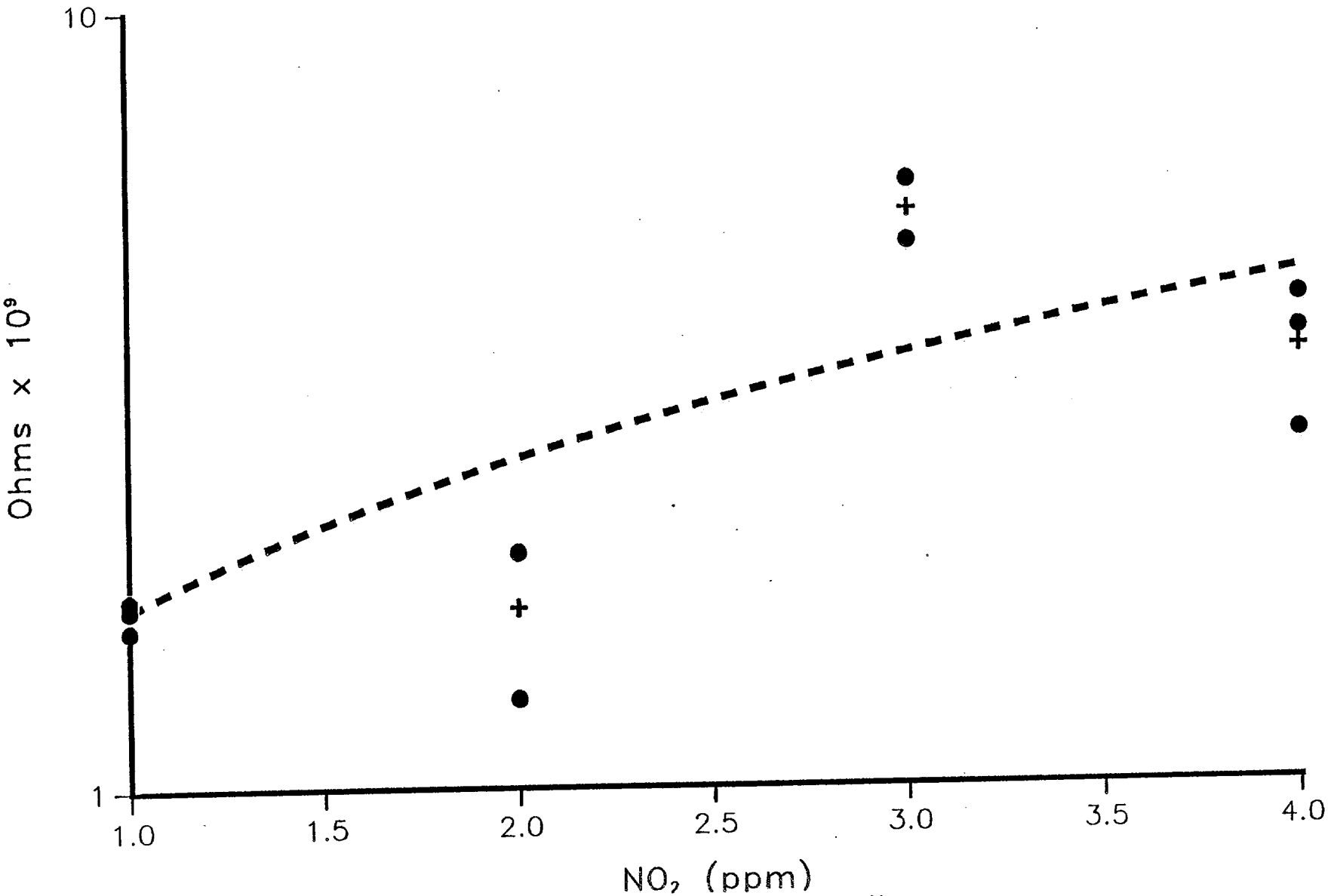

Figure 17. Effect of NO_2 on type B cell.

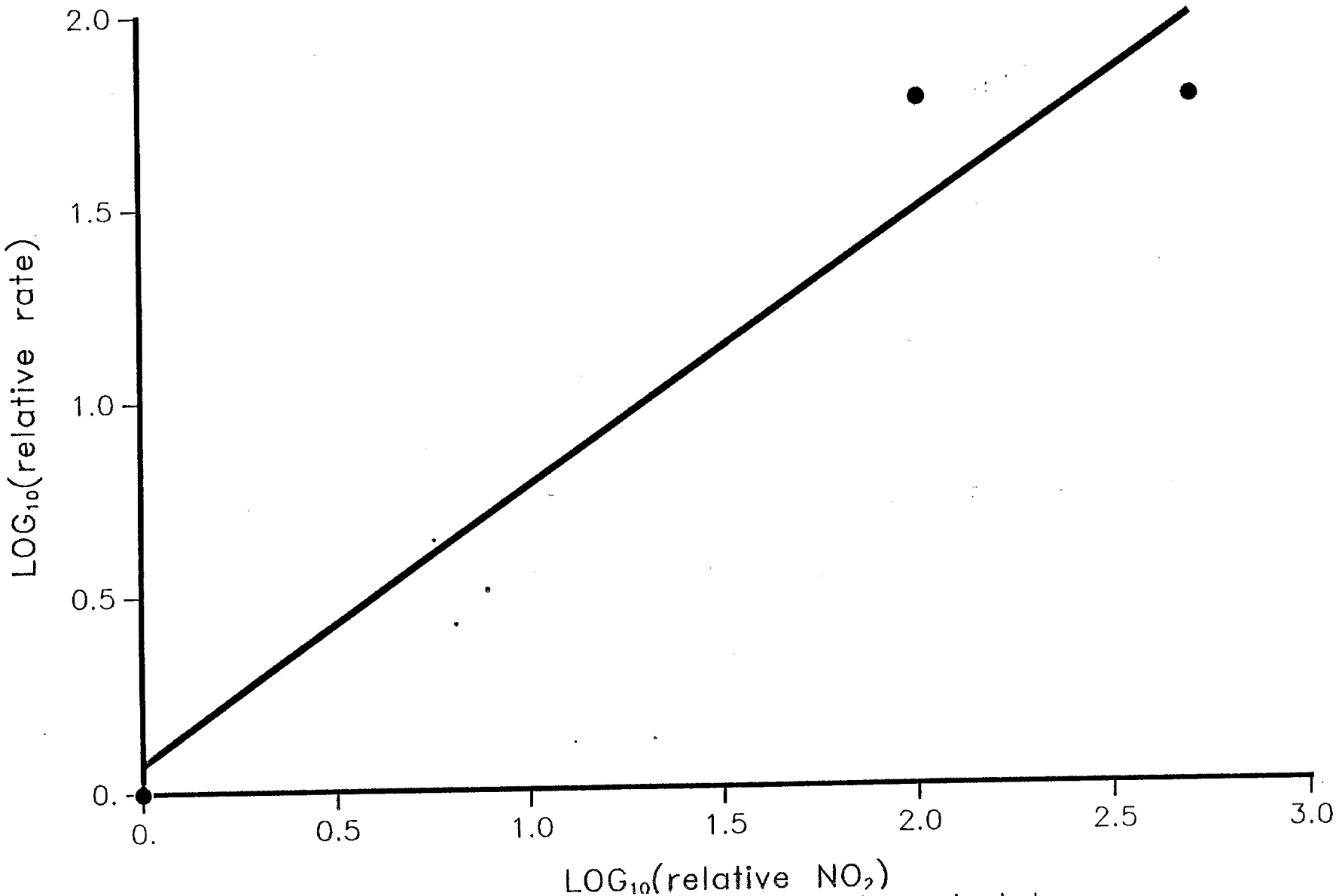

Figure 18. Order dependence from infrared data.

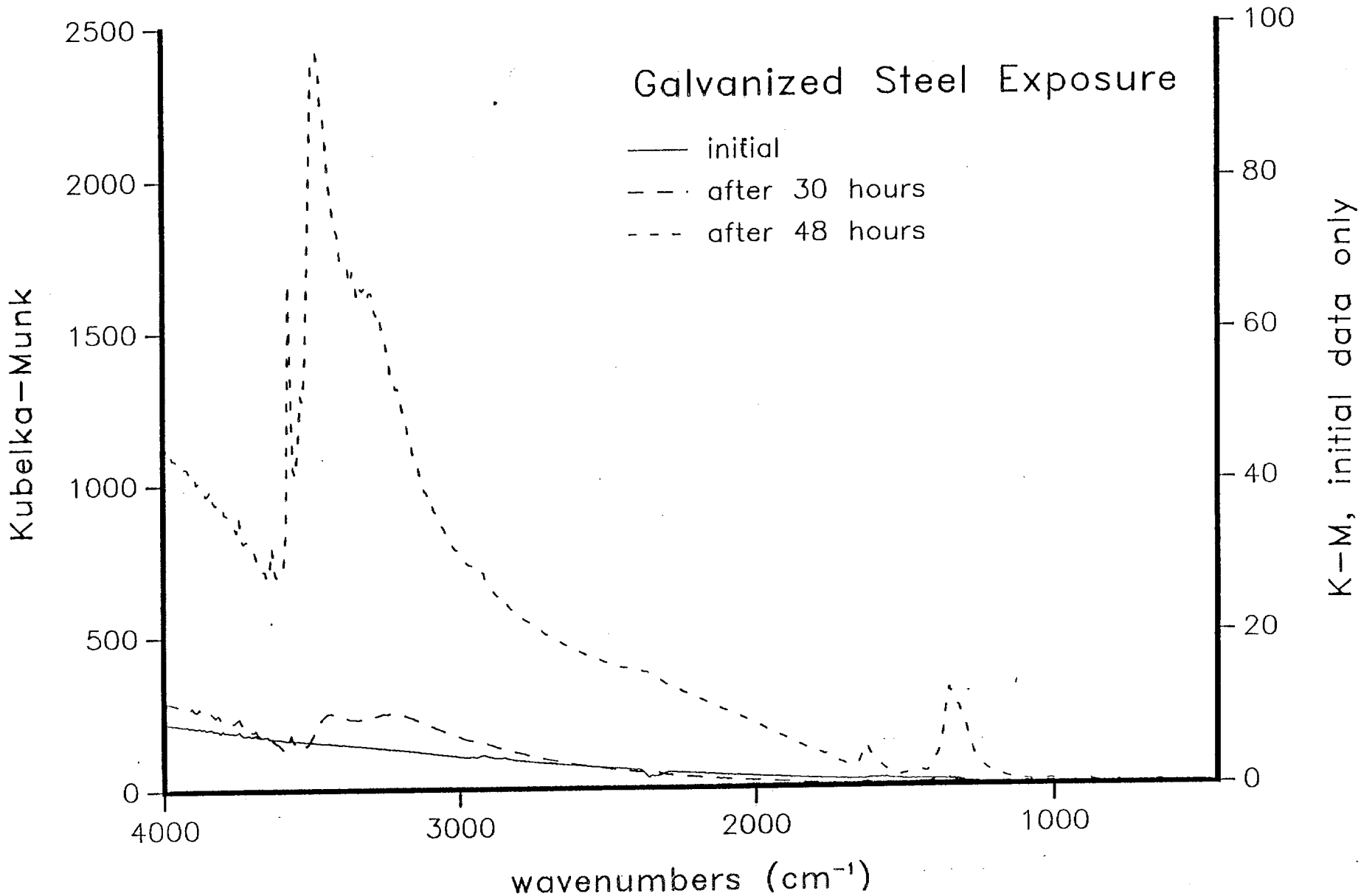

Figure 19. Corrosion products from Zn - HNO_3

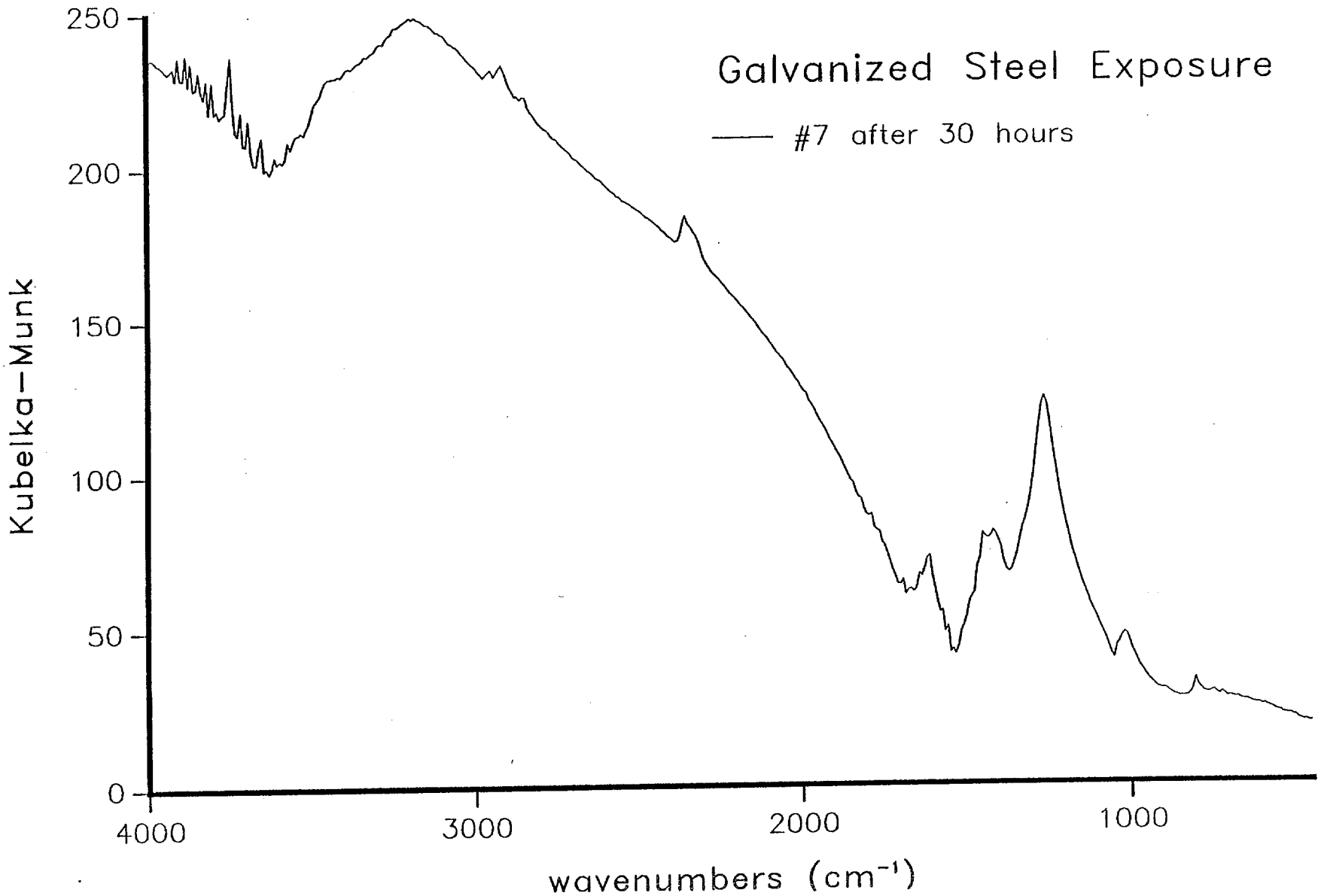

Figure 20. Corrosion products from Zn - HNO_3

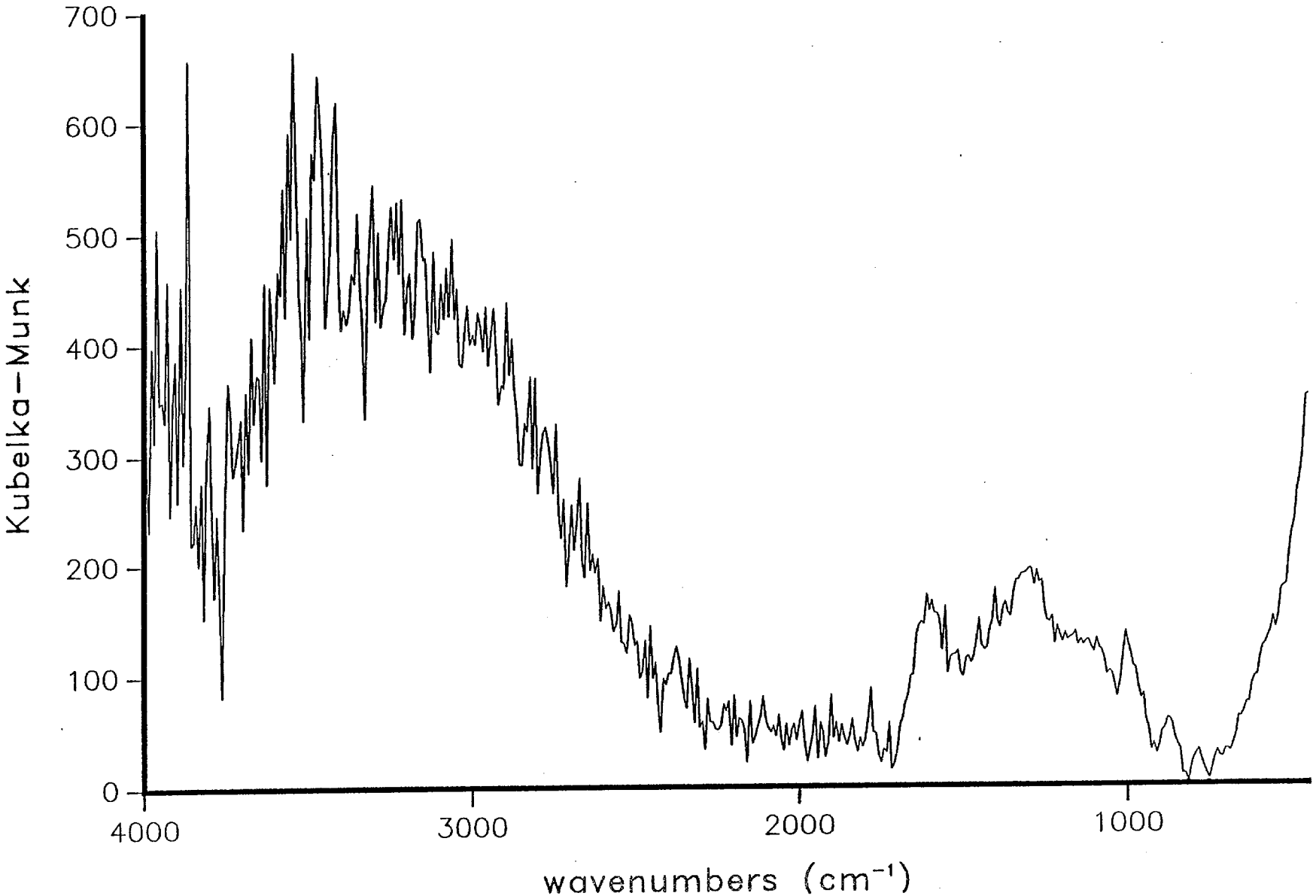

Figure 21. Corrosion products from Fe - HNO_3

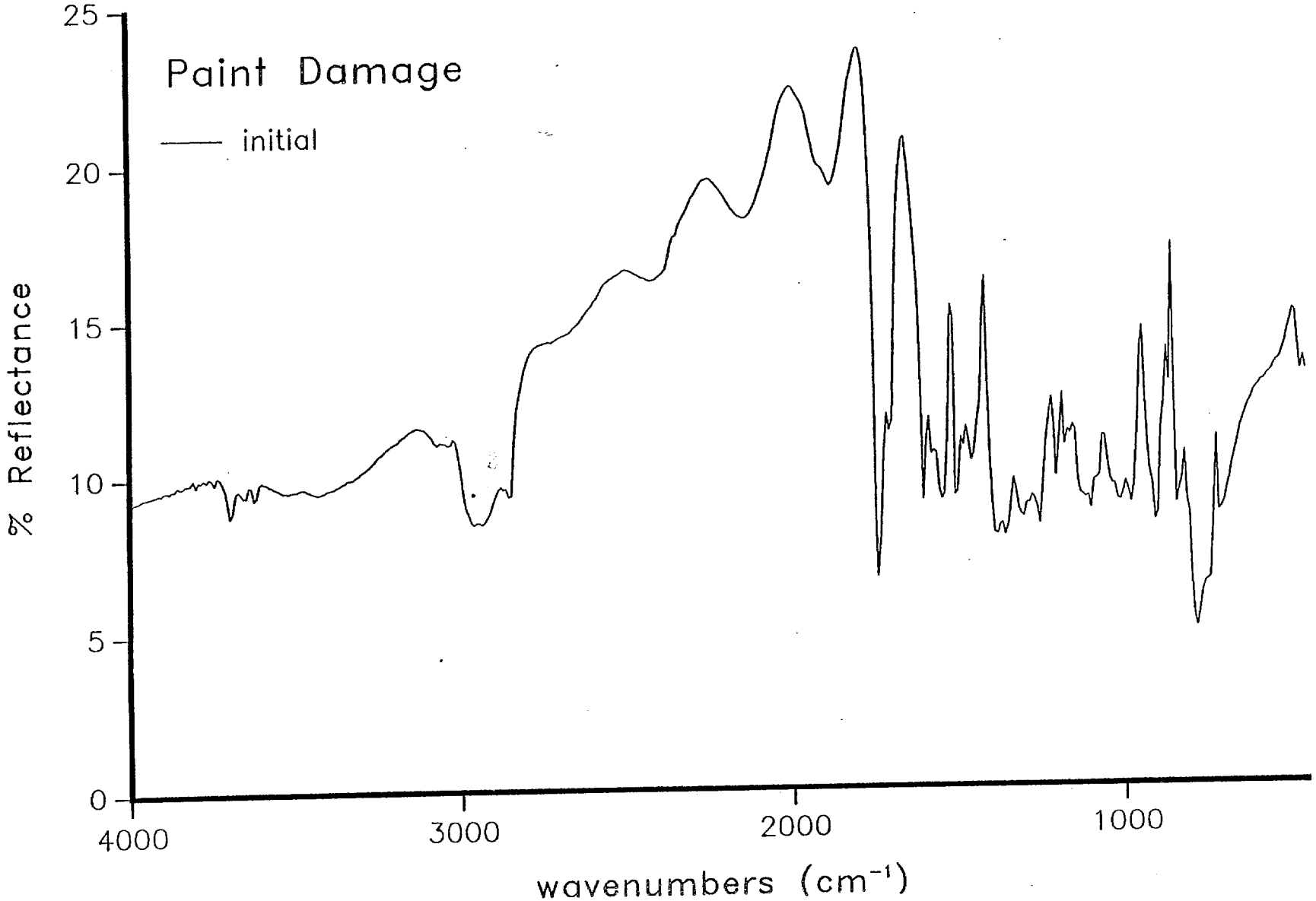

Figure 22. Corrosion of painted steel by HNO_3

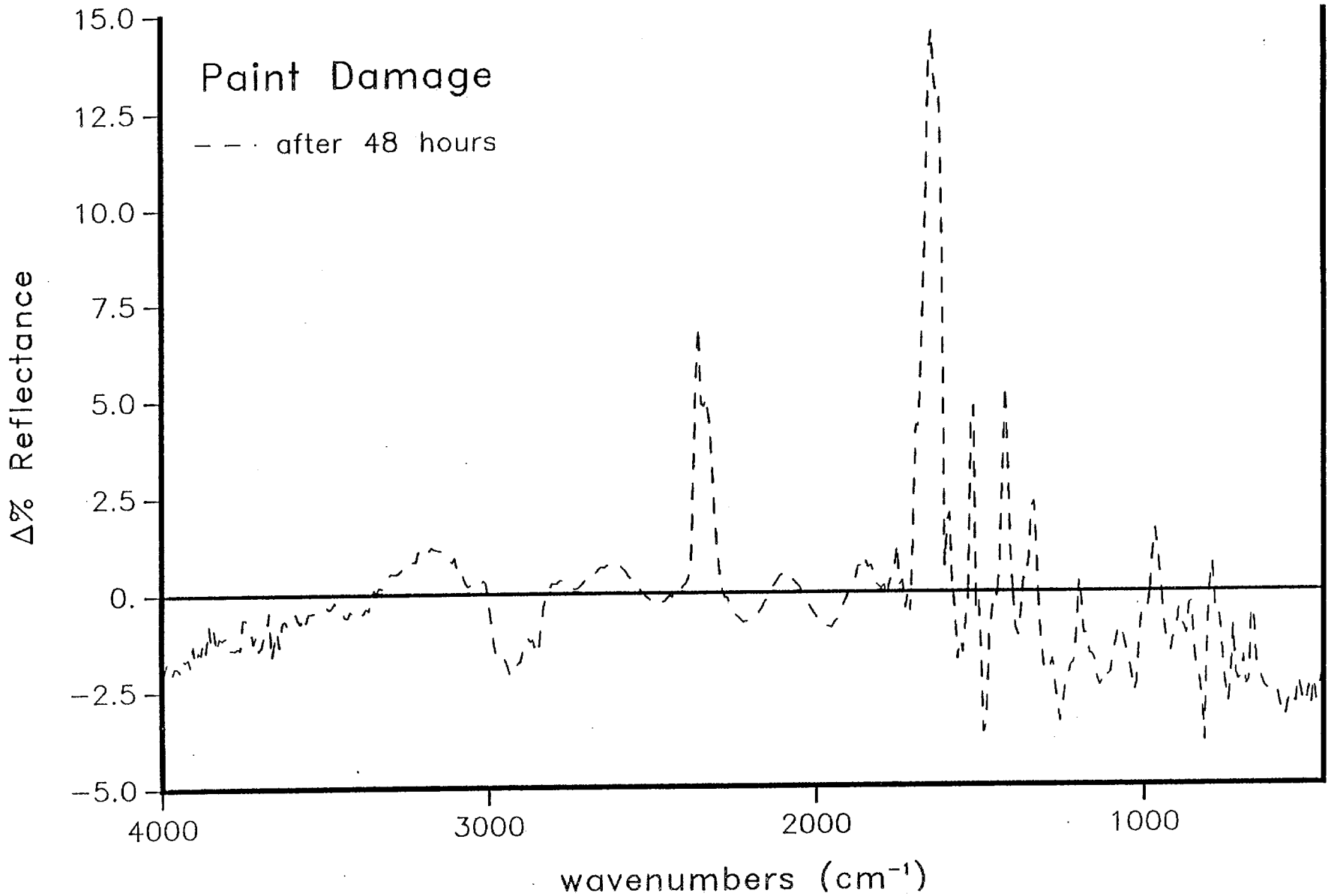

Figure 23. Corrosion of painted steel by HNO_3